Resource

Developmental Cell

In Vivo Developmental Trajectories of Human Podocyte Inform *In Vitro* Differentiation of Pluripotent Stem Cell-Derived Podocytes

Highlights

- scRNA-seq identifies distinct transcriptional profiles of human podocyte development
- Comparative analyses show similarities and differences of *in vitro*-derived podocytes
- Implantation study suggests vascular interactions improve *in vitro* podocyte maturation

Authors

Tracy Tran, Nils O. Lindström, Andrew Ransick, ..., Brendan Grubbs, Jill A. McMahon, Andrew P. McMahon

Correspondence

amcmahon@med.usc.edu

In Brief

Tran et al. performed single-cell RNA sequencing to provide an understanding of human podocyte development. Insights from the *in vivo* analysis was applied to extensively evaluate the formation of podocytes *in vitro*, highlighting autonomous programs of development and those requiring an interplay with adjacent cell types.

Tran et al., 2019, Developmental Cell *50*, 102–116
July 1, 2019
https://doi.org/10.1016/j.devcel.2019.06.001

CellPress

CellPress

Developmental Cell
Resource

In Vivo Developmental Trajectories of Human Podocyte Inform *In Vitro* Differentiation of Pluripotent Stem Cell-Derived Podocytes

Tracy Tran,[1] Nils O. Lindström,[1] Andrew Ransick,[1] Guilherme De Sena Brandine,[2] Qiuyu Guo,[1] Albert D. Kim,[1] Balint Der,[3] Janos Peti-Peterdi,[3] Andrew D. Smith,[2] Matthew Thornton,[4] Brendan Grubbs,[4] Jill A. McMahon,[1] and Andrew P. McMahon[1,5,*]

[1]Department of Stem Cell Biology and Regenerative Medicine, Broad-CIRM Center, Keck School of Medicine, University of Southern California, Los Angeles, CA 90089, USA
[2]Molecular and Computational Biology, Division of Biological Sciences, University of Southern California, Los Angeles, CA 90089, USA
[3]Department of Physiology and Neuroscience, Zilkha Neurogenetic Institute, Keck School of Medicine of the University of Southern California, Los Angeles, CA 90089, USA
[4]Maternal Fetal Medicine Division, University of Southern California, Los Angeles, CA 90089, USA
[5]Lead Contact
*Correspondence: amcmahon@med.usc.edu
https://doi.org/10.1016/j.devcel.2019.06.001

SUMMARY

The renal corpuscle of the kidney comprises a glomerular vasculature embraced by podocytes and supported by mesangial myofibroblasts, which ensure plasma filtration at the podocyte-generated slit diaphragm. With a spectrum of podocyte-expressed gene mutations causing chronic disease, an enhanced understanding of podocyte development and function to create relevant *in vitro* podocyte models is a clinical imperative. To characterize podocyte development, scRNA-seq was performed on human fetal kidneys, identifying distinct transcriptional signatures accompanying the differentiation of functional podocytes from progenitors. Interestingly, organoid-generated podocytes exhibited highly similar, progressive transcriptional profiles despite an absence of the vasculature, although abnormal gene expression was pinpointed in late podocytes. On transplantation into mice, organoid-derived podocytes recruited the host vasculature and partially corrected transcriptional profiles. Thus, human podocyte development is mostly intrinsically regulated and vascular interactions refine maturation. These studies support the application of organoid-derived podocytes to model disease and to restore or replace normal kidney functions.

INTRODUCTION

The functional unit of the kidney, the nephron, is made up of more than 14 distinct cell types (Lee et al., 2015). The most proximal component, the renal corpuscle, contains the glomerular filtration apparatus with the vascular endothelium ensheathed by podocytes in a three-dimensional network supported by mesangial myofibroblasts, encased by an outer capsule of parietal epithelium (McMahon, 2016). Within the renal corpuscle, podocytes extend foot processes, wrapping the glomerular vasculature, thus forming an interface for blood filtration. Podocytes are highly susceptible to damage during kidney injury, and genetic defects to podocytes frequently result in severe kidney disease (Greka and Mundel, 2012).

Recent progress has seen the publication of several directed differentiation protocols that generate complex associations of kidney-like cell types—kidney organoids—from pluripotent human stem cells (Freedman et al., 2015; Morizane et al., 2015; Taguchi et al., 2014; Takasato et al., 2014, 2015; Yamaguchi et al., 2016). Podocyte-like cells (PLCs) have been independently described several times in these systems (Kim et al., 2017; Sharmin et al., 2016). Data suggest PLCs develop along a process akin to that occurring *in vivo*. When transplanted either under the mouse kidney capsule or subcutaneously, PLCs attract and interact with mouse endothelial cells (ECs) (Bantounas et al., 2018; Van den Berg et al., 2018; Sharmin et al., 2016). Transcriptionally, PLCs, human glomeruli, and mouse podocytes partially overlap (Sharmin et al., 2016), and structurally, PLCs establish an apical-basal polarity resembling human capillary loop stage podocytes (Bantounas et al., 2018; Kim et al., 2017; Sharmin et al., 2016).

These findings suggest that pluripotent stem cell-derived PLCs have the potential for regenerative therapeutic approaches, disease modeling, and drug discovery; however, realizing this potential requires a strong understanding of normal podocyte development to optimize *in vitro* programs and to accurately assess PLC-derived cell types. To this end, we employed scRNA-seq to obtain a detailed picture of the *in vivo* program of human podocyte development. Comparison with *in vitro* PLC production demonstrates an extensive, but not complete, autonomous maturation in the absence of normal glomerular formation, with PLCs displaying vascular and mesangial organizing properties on transplantation beneath the mouse renal capsule. These data inform and support translational strategies with PLCs while highlighting areas where improvement is required to normalize PLC actions and properties.

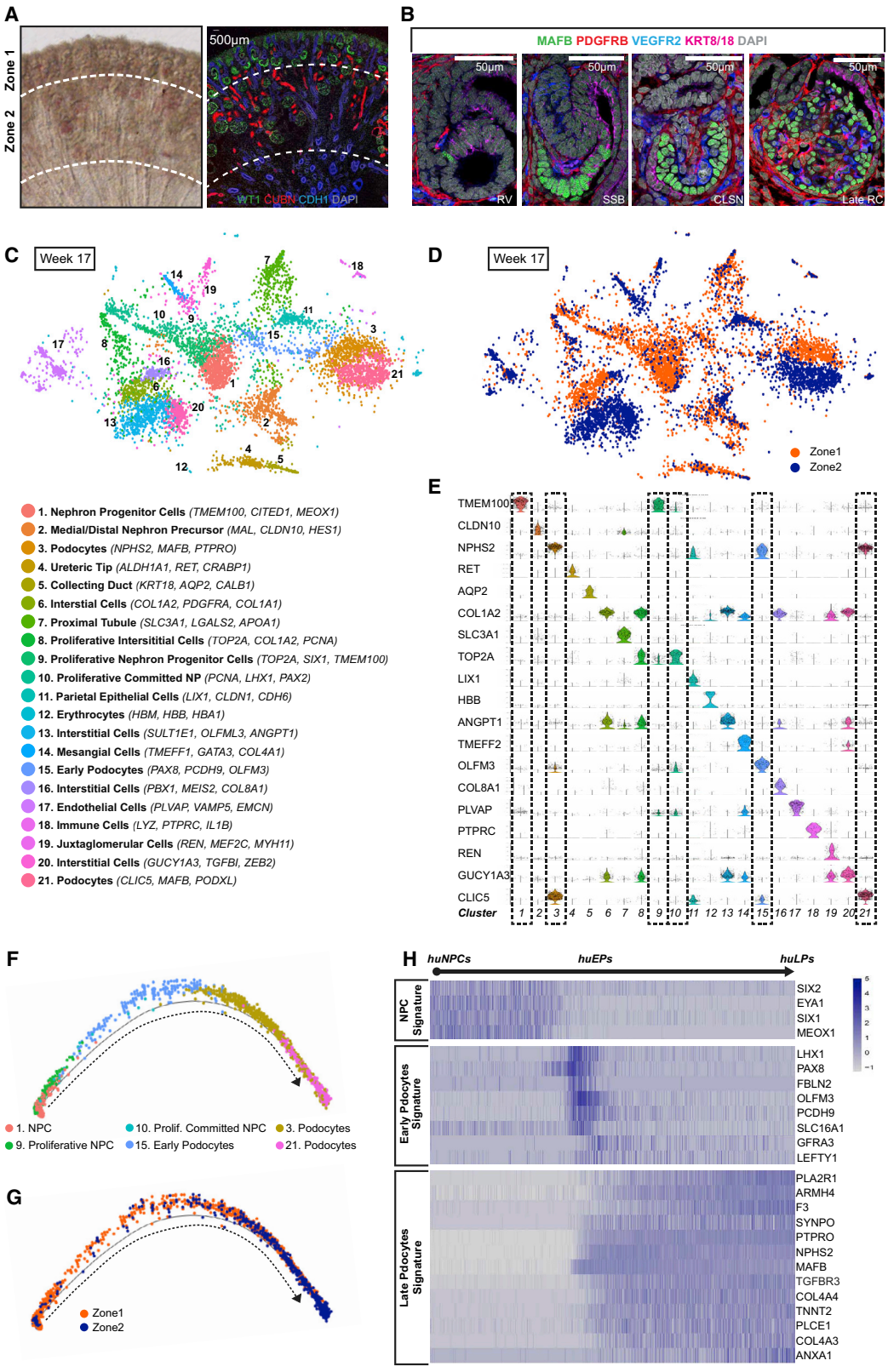

Figure 1. Single-Cell RNA-Seq Analyses Showing Transcriptional Changes during Differentiation of Human NPCs to Podocytes

(A) Left, Vibratome section of week 15–17 human fetal kidney containing zone 1 and zone 2 cells. Right, IF stain of a week 15–17 kidney cryosection highlighting mesenchymal progenitor cells, ureteric epithelial cells, early and late nephrons. Dotted lines indicated sites of microdissection to separate zone 1 and zone 2.

(legend continued on next page)

RESULTS

Single-Cell Transcriptomic Analysis of Human Nephrogenesis

Analysis of kidney organoids generated by the directed differentiation of pluripotent stem cells suggests organoid nephron-like structures resemble fetal and immature nephrons (Freedman et al., 2015; Morizane et al., 2015; Taguchi et al., 2014; Takasato et al., 2016). Given the lack of a comprehensive molecular framework for the formation of kidney cell types in the human fetal kidney, conclusions were limited and primarily founded on analysis of a few specific podocyte markers and selected morphological criteria.

We have begun to assemble a framework for the earliest stages of human nephrogenesis, within the cortical nephrogenic zone (Lindström et al., 2018a, 2018b, 2018c, 2018d; O'Brien et al., 2016). To extend these analyses to include more mature cell types, we performed scRNA-seq analyses on both the nephrogenic zone and the inner cortex. To preserve spatial information, we cut 300-μm thick vibratome sections of week 15–17 fetal kidney samples, manually dissected the outer nephrogenic cortex (zone 1) and the inner cortex (zone 2), and dissociated each region to enable scRNA-seq (using the 10× Chromium platform, as described previously in Lindström et al., 2018c) (Figure 1A).

Zone 1 and zone 2 cells enrich for early and late nephron cell types, respectively, and display contiguous transcriptomic signatures of nephron development. To visualize renal corpuscle developmental programs with a focus on podocyte development, we performed immunofluorescent analysis against specific proteins in zone 1 and 2 to distinguish podocytes (MAFB), ECs (VEGFR2), interstitial cells (PDGFRB), and epithelial nephron cell types (KRT8/18) in human fetal kidneys (Figure 1B). MAFB+ podocyte precursors emerged first in the proximal segment of the renal vesicle (RV). As the RV matures to comma-shaped body (CSB) nephrons and the glomerular cleft forms and expands, cuboidal podocyte precursors lie on the proximal side of the glomerular cleft. Endothelial and interstitial cells invaded the glomerular cleft at the CSB stage and were likely progressively recruited during the transition to the S-shaped body (SSB) stage, as podocyte precursor cells extended along the length of the glomerular cleft (Figure 1B). The RV to SSB progression was limited to zone 1. In zone 2, nephrons matured to the capillary loop stage (CLSN) and functional filtering nephrons. The progressive development of the renal corpuscle is highlighted by the interplay among podocytes (MAFB+), ECs (VEGFR2+), and mesangial cell population (PDGFRB+) as these cell types expand, rearrange, and mature to form the renal filtration unit (Figure 1B).

Zone 1 and 2 scRNA-seq profiles from a week 17 human kidney were subjected to quality control filtering, and 7,518 single-cell transcriptional profiles were merged into one dataset. Cell groupings were identified by unsupervised clustering using a Gaussian mixture model (Lindström et al., 2018d; Scrucca et al., 2016). Twenty-one clusters emerged from this analysis (Figure 1C). Each cluster was identified by the expression of known human kidney cell type markers (Lindström et al., 2018a, 2018b, 2018c, 2018d) (Figures 1C and 1E) (Table S1). Following expectations, zone 1 was enriched for early progenitor and differentiated cell types from the nephrogenic, interstitial, and ureteric lineages, whereas zone 2 consisted of more mature cell types (Figures 1C, 1D, and S1E). ECs were identified in both zone 1 and zone 2, while mesangial cells (MCs) predominated in zone 2 (Figures 1C, 1D, and S1E). Cell cluster identification suggested a continuum of nephrogenic lineage cell progression from nephron progenitor cells (NPCs) to maturing nephron cell types.

As we also aimed to examine the presence of glomerular vascular and MCs in the *in vitro* culture, signatures of these two cell types were identified from the scRNA-seq datasets. We confirmed that coexpression of PDGFRB and GATA3 marked the pericytes recruited to renal corpuscles, and committed MCs in late RC coexpressed *GATA3* and *TMEFF2* (Figures S4A, 5G, and 5H). Human glomerular vascular cells activated *PECAM1*, *EHD3,* and *GATA5* (Figures 5I and S4A), and *GATA5* expression was also detected in the mouse glomerular vasculature (Messaoudi et al., 2015) (Figure 5K).

To validate key predictions from the week 17 kidney analysis, we performed scRNA-seq on a week 15 kidney sample. The 6,129 zone 1 and 2 scRNA-seq profiles formed 21 clusters (Figures S1A–S1D). Although the proportion of cells varied within clusters at week 15 and week 17, as expected, the cell type diversity was similar. Overall, the scRNA-seq quality was stronger in the week 17 sample, and to avoid a loss of resolution in more detailed studies of the podocyte, we focused on this sample for further analysis.

Establishing the Developmental Trajectory from Nephron Progenitor to Human Podocyte

To identify normal transcriptional changes in the podocyte forming program, we selected 3,318 cells including: NPCs (clusters 1 and 9), proliferative developing nephron cells (cluster 10), early podocytes (cluster 15), and maturing podocytes (clusters 3 and 21). Monocle 2.0 was used to assemble data into a predicted developmental trajectory (Figures S2A, S2B, 1F, and 1G). One end point of the trajectory comprised nephron progenitors (B1), and the other podocytes (B2) with a side branch of

(B) IF stain showing morphogenesis of the renal corpuscle through RV, SSB, CLSN, and late RC stages.
(C) Unsupervised clustering of week 17 kidney cells from both zone 1 and zone 2 displayed in a tSNE plot with annotation of cluster identities. In parentheses are differentially expressed genes used for cluster identification.
(D) tSNE plot of week 17 kidney cells colored by their original zonal identities.
(E) Violin plots of differentially expressed genes used to classify 21 clusters. Dotted-lined boxes mark uncommitted, committed NPC and podocyte clusters subjected to secondary analyses.
(F) Pseudotime trajectory from NPC to podocytes after removal of cells with strong cell-cycling signature. Cells are colored by their cluster identities.
(G) Pseudotime trajectory from NPCs to podocytes with cells colored by their original zonal identities.
(H) Heatmaps of selected genes whose expression changes along the differentiation trajectory from NPCs to podocytes.
RV, renal vesicle; SSB, S-shaped body nephron; CLSN, capillary loop stage nephron; Late RC, late renal corpuscle; huNPC, human nephron progenitor cell; huEP, human early podocyte; huLP, human late podocyte.

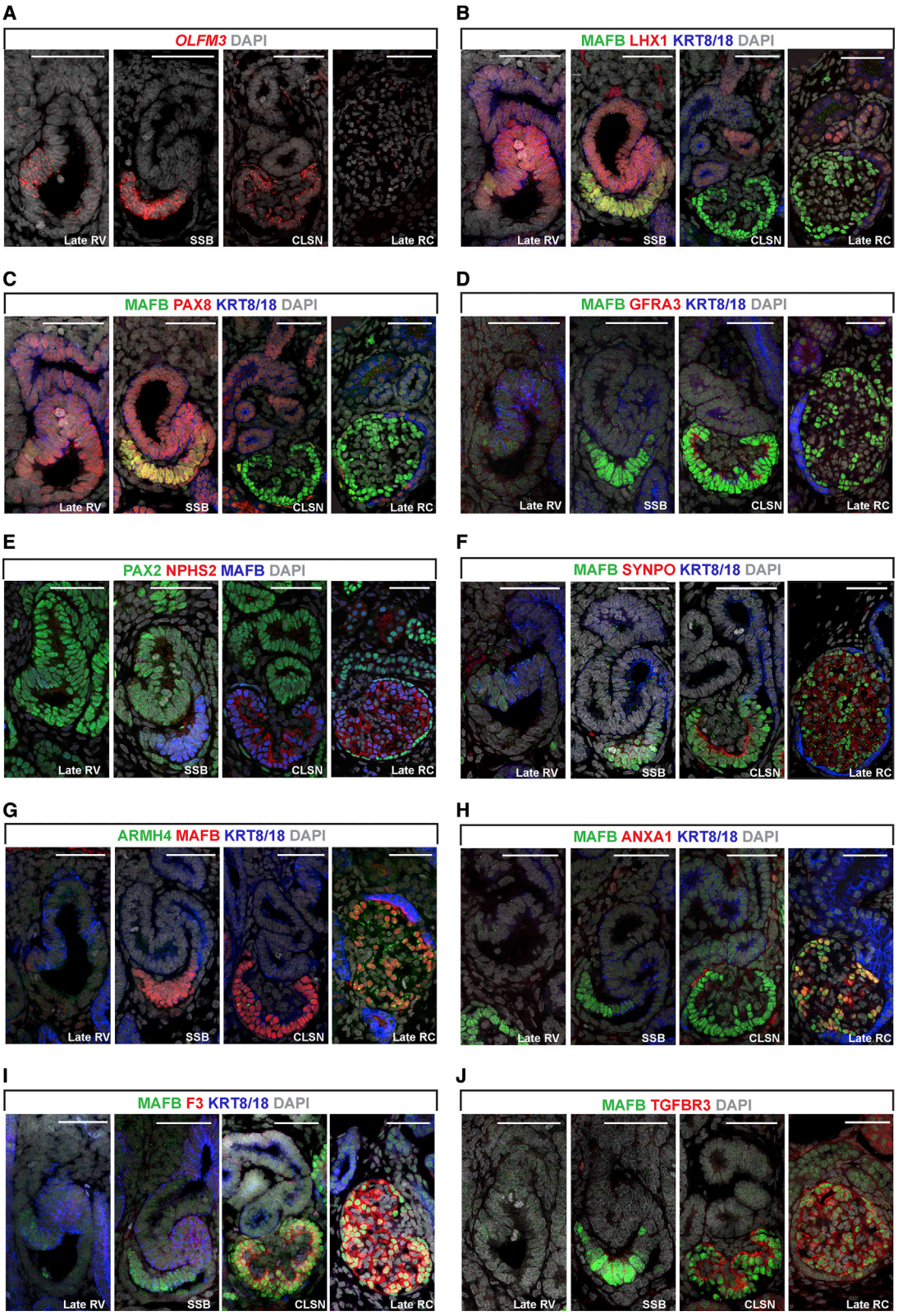

(legend on next page)

proliferating cells, collectively grouped by a strong cell cycle signature (branch B3) (Figure S2C). A second iteration of pseudotime analysis was performed from NPCs to podocytes (2,705 cells of branches B1 and B2). As expected, zone 1 and zone 2 cells concentrated at either ends of the trajectory (Figure 1F). NPC genes such as *SIX1, SIX2*, *EYA1,* and *MEOX1* were present at the start of the trajectory and downregulated along the predicted developmental progression. The loss of an NPC signature corresponded to the onset of a podocyte signature. A cohort of genes predicted to display a distinct transient early podocyte (EP)-restricted activity (including *LHX1, PAX8, FBLN2, OLFM3*, *PCDH9*, *SLC16A1*, *GFRA3*, and *LEFTY1*) gave way to a late podocyte (LP) gene expression signature (including *PLA2R1, ARMH4, F3, SYNPO, NPHS2, MAFB, TGFBR3, COL4A3, COL4A4, TNNT2*, *PLCE1,* and *ANXA1*) (Figure 1H). Analysis of week 15 and 17 scRNA-seq confirmed EP and LP signatures within zones 1 and 2, respectively (Figures S1F and S1G).

We generated comprehensive human EP (huEP) and LP (huLP) signatures by identifying genes whose expression correlated with representative EP and LP signatures (Figure S2D), and examined their expression along the human podocyte developmental trajectory (Figure S5) to generate curated lists of 158 EP and 104 LP signature genes. Among the EP genes, about half were activated in NPCs. Many of these were enriched in uncommitted and committed NPCs (red text, underlined; Figure S5), and were upregulated in the early period of podocyte development (Figure S2E). Seventy-five genes were transiently expressed in a narrow window of EP development including a number of genes known to control or demarcate nephron induction (green text, underlined; Figure S5) (Figure S2E). Interestingly, 40 EP genes encoded ribosomal proteins (“RPL” or “RPS” genes) downregulated at the initiation of podocyte development. The LP signature list included genes encoding transcription factors known to regulate podocyte development, cytoskeletal components, and extracellular matrix proteins linked to glomerular function (Figure S2F). Many EP (*CCND1*) and LP (*CD151, GSN, COL4A4, THSD7A, NPHS2, CLIC5, VEGFA, PLA2R1, COL4A3, CTGF*, and *MAFB*) genes have been associated with genetic disorders of the glomerulus or kidney (Figure S2K) (Online Mendelian Inheritance in Man, 2018). We confirmed the expression of 72/104 LP genes in adult podocytes using the Human Protein Atlas, highlighting their relevance as a mature podocyte signature (Uhlen et al., 2010, 2015) (Table S2).

To determine whether human podocyte differentiation is conserved in the mouse, we compared the human EP and LP signatures with the mouse microarray analyses of Mafb-GFP+ podocytes from E13.5 embryos and adult kidneys (Brunskill et al., 2011). Our analyses suggested a modest overlap between the two species, with 13 EP and 40 LP genes shared between mouse and human (Figures S2G and S2H), many of which have been described to be important for mouse podocyte morphogenesis (discussed later).

We pinpointed when in podocyte development EP and LP gene profiles were established by combining immunofluorescent detection of target protein, or RNAscope fluorescent *in situ* hybridization to a target mRNA, on sections of 15- to 17-week human fetal kidneys. RV and SSB podocyte precursors expressed EP markers (*OLFM3*, PAX8, and LHX1) but expression ceased prior to or at CLSN stages (Figures 2A–2C). GFRA3 expression was restricted to CLSN podocytes (Figure 2D). We also examined the expression of *RPS21*, encoding Ribosomal Protein S21, using *in situ* hybridization and observed lower activity in mature renal corpuscle podocytes (Figures S2I and S2J). LP markers (NPHS2, SYNPO, ARMH4, ANXA1, F3, TGFBR3, PLA2R1, COL4A3, and TNNT2) were first detected in SSB or CLSNs, and the highest levels were observed in mature renal corpuscles (Figures 2E–2J, S4E, and S4F). Interestingly, ANXA1, which is only expressed in the late RC stage, displayed a unique distribution with markedly varying levels in individual podocytes within a single renal corpuscle (Figure 2J). Based on these observations, we estimated the expression windows of EP and LP genes, and categorized them into smaller groups. EP signature genes can be separated into those activated in NPCs and early committed NPCs (group EP1), those activated in RV and highly expressed in SSB-stage podocyte precursors (group EP2), and those transiently expressed in the CLSN podocytes (group EP3) (Figure S5). LP genes maintained high expression levels in late RC-stage podocytes, but can be divided into the early- and late-activated groups (groups LP1 and LP2, respectively) (Figure S6).

In summary, the single-cell transcriptome profiles define the molecular development of the human podocyte lineage providing a molecular framework for analyzing development of PLCs *in vitro*.

Transcriptomic Profiling of PLCs Generated from MAFB-Reporting hESCs

To facilitate analysis of *in vitro*-derived PLCs, we generated a MAFB-P2A-eGFP H9 hESC line that places eGFP under the control of the *MAFB* gene (Figure S3A). *MAFB* encodes a key transcriptional regulator of podocyte gene expression that has been shown to play a critical role in mouse podocyte development (Sadl et al., 2002). Expression of the mouse and human gene can be detected in podocyte precursors as early as the RV stage (Figures 1B and 2A–2J) and MAFB activity continues into mature podocytes in both the adult mouse and human fetal kidney (Lindström et al., 2018a).

MAFB-P2A-eGFP H9 hESCs were differentiated into kidney organoids using existing protocols (Morizane et al., 2015) with minor modifications (Figure 3A). Whole organoid transcriptional profiling at differentiation day (DD) 0, 8, 10, 16, 22, and 28, guided by parallel immunofluorescent analysis with informative markers, showed induction and differentiation of characteristic nephron cell types in the kidney organoids (Figures S3B and S3C). eGFP+ cells first appeared at DD 13-14 with a subsequent

Figure 2. *In Vivo* Validation of Early and Late Podocyte Signatures

(A) Fluorescent *in situ* hybridization showing expression of EP gene *OLFM3* in RV, SSB, CLSN and late RC stages. Scale bars: 50 μm.

(B–J) IF stains of EP markers (LHX1, PAX8, and GFRA3), and LP markers (NPHS2, SYNPO, ARMH4, ANXA1, F3, TGFBR3, and MAFB) showing their expression in RV, SSB, CLSN, and late RC stages. Scale bars: 50 μm.

RV, renal vesicle; SSB, S-shaped body nephron; CLSN, capillary loop stage nephron; Late RC, late renal corpuscle; EP, early podocyte; LP, late podocyte.

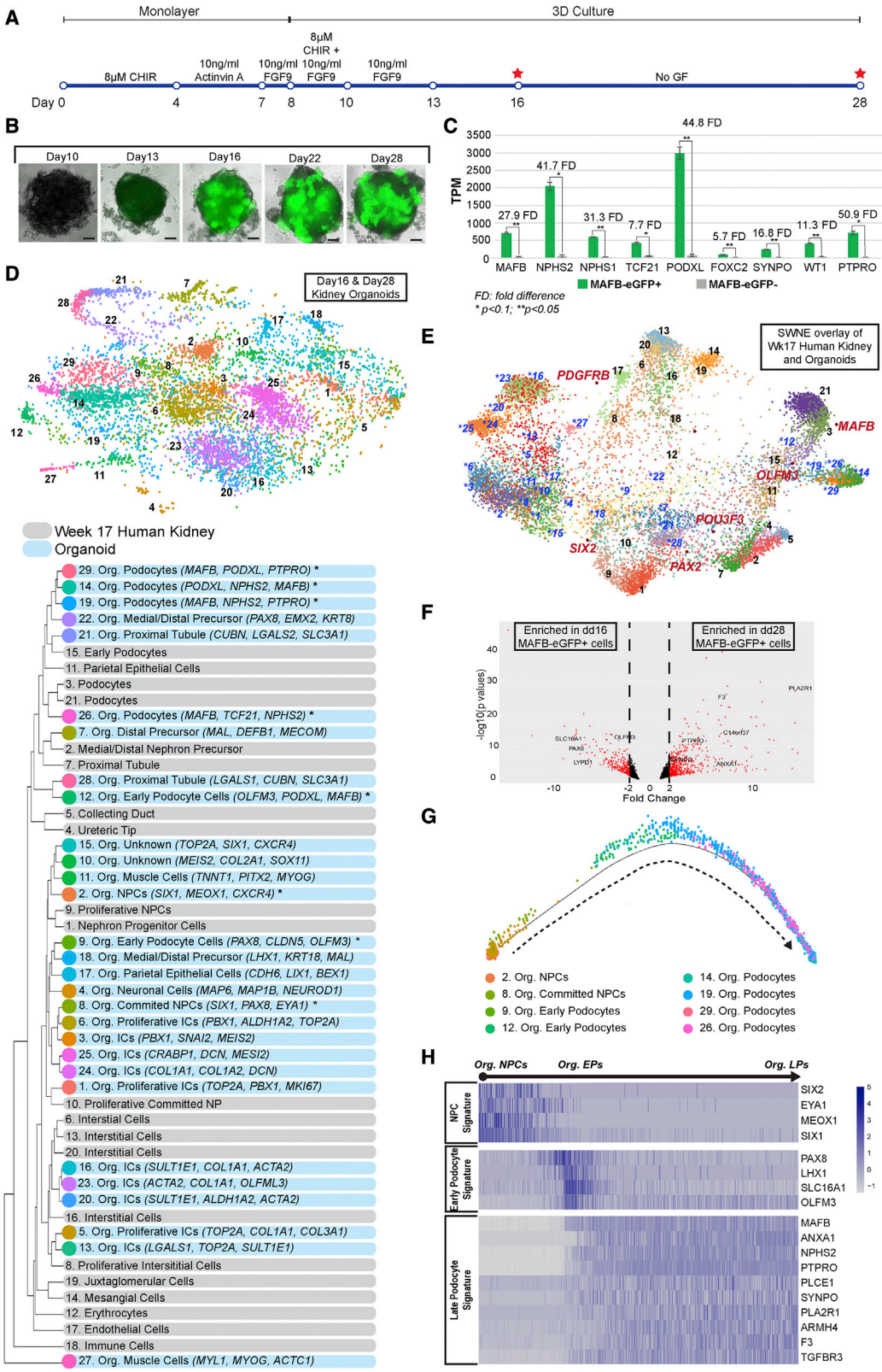

Figure 3. Single-Cell RNA-Seq Analyses Showing Transcriptional Changes during *In Vitro* Derivation of Podocytes

(A) Schematic diagram summarizing the 28-day protocol to generate kidney organoids from human ESC. Red stars denote the time points selected for further analyses using scRNA-seq.

(legend continued on next page)

increase in both the numbers of eGFP+ cells and the level of eGFP fluorescence to DD 28 (Figure 3B). As expected, the eGFP signal was tightly correlated with endogenous MAFB activity and colocalized with WT1, a known determinant of podocyte programs (Berry et al., 2015; Chau et al., 2011; Gebeshuber et al., 2013; Hammes et al., 2001; Kann et al., 2015; Moore et al., 1999) (Figure S3D). RNA-seq profiling of FACS-isolated MAFB-eGFP+ cells from DD 28 organoids confirmed significant enrichment of MAFB and other podocyte marker genes (Figure 3C). Further, hierarchical clustering of eGFP+ cells with human fetal renal corpuscles, immortalized podocytes (imPod) before and after thermoswitch emphasized improved resemblance of hESC-derived podocytes to the *in vivo* cells, supporting their use as a markedly enhanced tool for *in vitro* studies (Figure S3F). Additionally, gene ontology (GO) analysis highlighted podocyte-related terms (Figure S3E). Collectively, these data demonstrate that the eGFP+ labeling strategy specifically identifies PLCs in kidney organoid culture.

To investigate whether PLCs develop along a similar trajectory to human fetal podocytes, we performed scRNA-seq on organoids at DD16 and DD 28 (2,153 cells from DD 16, and 5,818 cells from DD 28). These two time points were selected as organoids strongly expressed EP signatures (including *PAX8, OLFM3, LYPD1,* and *SLC16A1*) at DD 16, and mature nephron signatures (including *F3, PTPRO*, *C14orf37* or *ARMH4, SYNPO, ANXA1*) at DD 28 (Figure S3C). After quality control filtering, unsupervised clustering of scRNA profiles for 7,200 organoid cells assigned this population to 29 groups (Figures 3D and S3G). Each of these was identified through expression of marker genes, and hierarchical clustering was performed to match these groupings with the most closely related clusters of the week 17 human kidney scRNA-seq (Figure 3D). Similarity Weighted Nonnegative Embedding (SWNE) analysis (Wu et al., 2018b) of the *in vivo* and *in vitro* cells merged object concurred with the hierarchical clustering and confirmed our identifications of *in vitro* cell types (Figure 3E).

Organoids comprised cells with transcriptional signatures indicative of interstitial cells (*COL1A1+, ALDH1A2+*), nephron progenitors (*SIX1+*, *MEOX1+*), early developing nephron cells (*PAX8+*, *LHX1+*), precursors of the medial/distal segment (*SOX9+*, *MECOM+*, *EMX2+*), proximal tubule (*LRP2+*, *SLC3A1+*), parietal epithelial cells (*LIX1+, CDH6+*), and early and LPs (*OLFM3+*, *MAFB+*, *NPHS2+*). Two clusters unexpectedly expressed muscle markers (*MYOG+, MYL1+*) and another cluster displayed a prominent neuronal signature (*MAP6+, NEUROD1+*) supporting recent observations of lineage heterogeneity in kidney organoid protocols (Czerniecki et al., 2018; Wu et al., 2018a). Two clusters (10 and 15) with mixed but incomplete NPC and IC signatures were left "unidentified". Of note, organoids are devoid of vascular cells precluding vascular podocyte interactions in podocyte development *in vitro*.

To examine the PLC lineage more specifically, we identified 2,188 cells with NPC-like or PLC signatures and predicted developmental trajectories between the cell types (Figures S3H and S3I). As branch 3 (B3) contained mostly mitotic cells, we focused on the differentiation trajectory from organoid NPCs to PLCs of 1,941 B1 and B2 cells (Figures S3G–S3J). We observed similar transcriptional changes to those identified in human podocyte development. EP signature genes (including *OLFM3*, *PAX8*, *LHX1,* and *SLC16A1*) were transiently upregulated as NPC signature genes were deactivated, and downregulated when LP signature genes (including *ANXA1, NPHS2, PTPRO, PLCE1, SYNPO, PLA2R1, ARMH4, F3,* and *TGFBR3*) were upregulated (Figure 3H). EP and LP genes were also enriched in DD 16 and DD 28 MAFB-eGFP+ cells, respectively, in bulk RNA-seq analyses (Figure 3F). Immunofluorescent analysis of EP and LP-associated proteins within PLCs at DD 16 and DD 28 confirmed the EP to LP gene expression transition (Figures 4A–4F). In summary, PLCs follow a developmental trajectory similar to that observed in human podocyte development: DD 16 PLCs resemble podocytes in SSBs while DD 28 PLCs are similar to podocytes of the CLSN or later stages.

Comparison of PLCs and Human Podocytes

To determine the overlap between PLCs and human podocytes, we performed differential expression gene test between their transcriptomes (Figure 4G) (Table S1). Of the previously identified EP and LP signature genes in the fetal kidney, most of these (137 EP genes and 84 LP genes) followed a similar early-late developmental time course *in vitro* (Figures S6). LP genes were absent, or expressed at low level, including genes encoding key extracellular matrix components linked to kidney disease (including *COL4A3*, *COL4A4*) and angiogenic factors (including *CXCL12, EFNB1*) (Figures 4G, 4H, and S6) (Table S2). Among the EP genes, we validated the expression of *OLFM3* and GFRA3 in DD 28 podocytes by *in situ* hybridization and immunofluorescence, respectively (Figures 5D and 5F). We also observed coexpression of EP (GFRA3) and LP genes (ANXA1) in DD 28 MAFB+ cells (Figures 4J and 5F). While GFRA3 and ANXA1 were detected at distinct stages of *in vivo* podocyte development,CLSN and late RC respectively (Figures 2D, 2H, and 4I), coexpression in DD 28 organoids showed the

(B) Bright-field and (gray scale) endogenous eGFP (green) imaging of the kidney organoids after transition to 3D cultures. Scale bars: 200 μm.
(C) RNA expression levels of known podocyte markers in MAFB-eGFP+ cells versus MAFB-eGFP- cells. Statistical significance is determined using Student's t test.
(D) Top, unsupervised clustering of cells from DD 16 and DD 28 presented in a tSNE plot.
Bottom, annotation of organoid cluster identities and differentially expressed genes used for cluster identification. Hierarchical clustering suggested relationship among organoid cell clusters and human week 17 cell types. Asterisks (*) mark organoid NPC and podocyte clusters selected for secondary analyses using *Monocle 2.0*.
(E) SWNE overlay of week 17 human kidney and organoid clusters. Black numbers: week 17 human kidney clusters; Blue numbers (with asterisks): organoid clusters. "Factor genes" in red are known kidney cell type markers.
(F) Volcano plot with annotations of selected genes that were differentially expressed between DD 16 and DD 28 MAFB-eGFP+ cells.
(G) Pseudotime trajectory from organoid NPCs to podocytes with cells colored by their cluster identities.
(H) Heatmaps of selected genes whose expression changes along the differentiation trajectory from organoid NPCs to podocytes.
Org, organoid; NPC, nephron progenitor cell; IC, interstitial cell; DD, differentiation day; EP, early podocyte; LP, late podocyte.

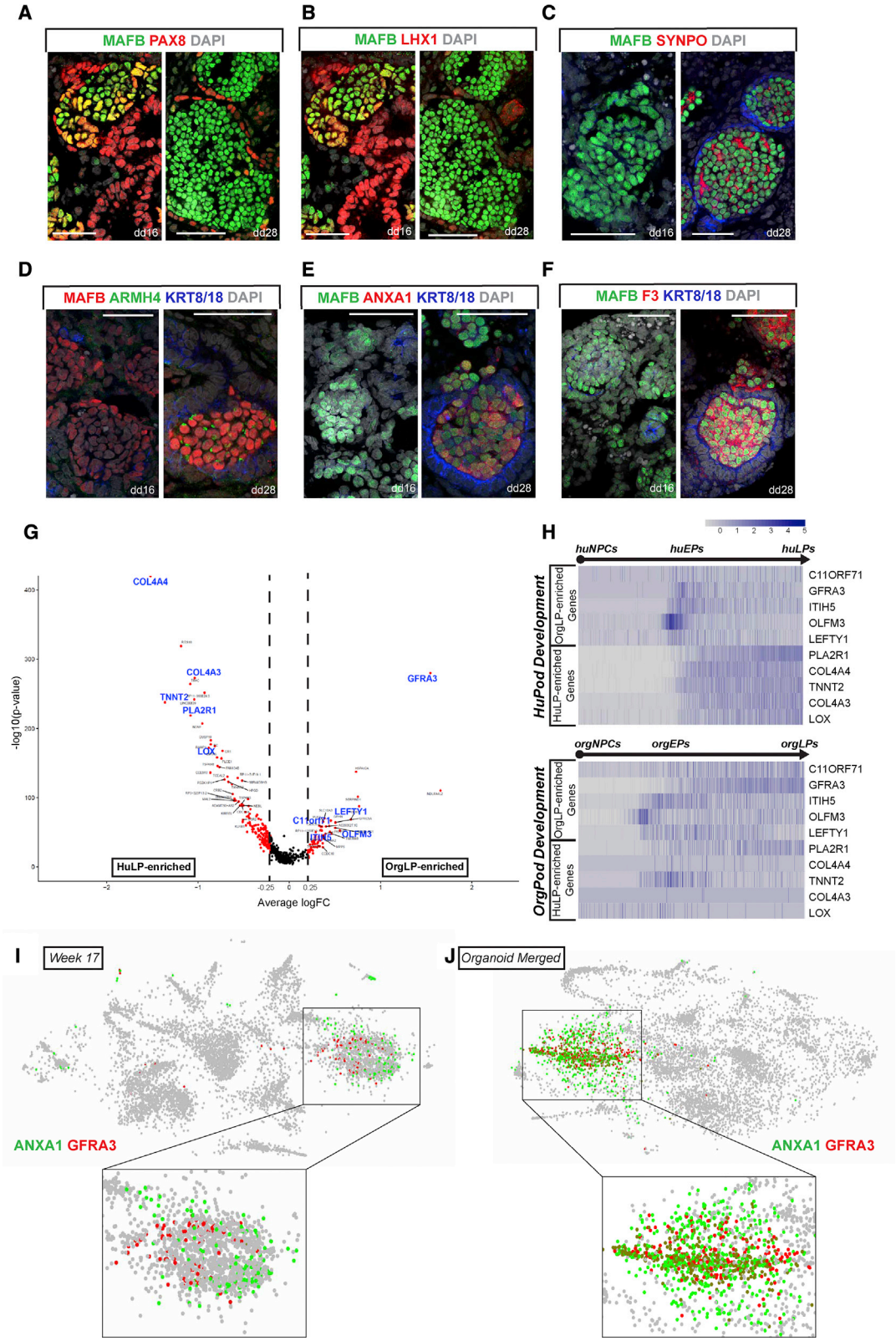

Figure 4. Comparison of *In Vitro*-Derived Podocytes to Human Podocytes

(A–F) IF stains to validate expression of EP markers (PAX8 and LHX1) and LP markers (SYNPO, ARMH4, ANXA1, and F3) in DD 16 and DD 28 organoid podocytes. Scale bars: 50 μm.

(legend continued on next page)

down-regulation of EP signature genes was incomplete. DD 28 organoids were a mosaic of EP-like (e.g. GFRA3+ANXA1-) and LP-like (e.g. GFRA3-ANXA1+) cell types (Figures 4J and 5F). Further, some LP genes including *TNNT2, TNNI1, CAPN2, DCN, IGFBP7, CTGF*, *CXCL12*, and *CYR61* were weakly active in DD 16 podocytes, but subsequently downregulated in DD 28 PLCs (see *TNNT2* in Figure 5E). An examination of published scRNA-seq profiling of kidney organoids (Czerniecki et al., 2018; Wu et al., 2018a) also suggests similar misexpression of EP and LP genes in other organoid datasets in the literature, indicating the observations here are likely of broad relevance to *in vitro* organoid models (Figures S4C and S4D).

Collectively, these findings show a surprising level of maturation of *in vitro*-derived podocytes that is independent of the vascular and mesangial components, and pinpoint aspects of *in vitro* podocyte programing for further improvement.

Examination of Glomerular Disease-Relevant Genes

To examine the applicability of *in vitro* derived podocytes to glomerular disease studies, we examined expression of genes associated with human glomerulosclerosis and glomerulopathy in the human glomerular cell types (Lepori et al., 2018, Online Mendelian Inheritance in Man, 2018). Forty-three genes were expressed in all three glomerular components: *LMNA, COL4A1, MPV17*, *KANK2*, and *MYO1E* were more highly expressed in the MCs, while *DGKE, KHDRBS3, SOX18, SLC7A7*, *KANK4*, and *TAL1* were enriched in the endothelial component. Of the 12 genes activated in podocytes, *PAX2* and *FAH* were upregulated only in EPs, while *PTPRO, COL4A3, COL4A4, PLCE1, CRB2, NPHS1, TCF21*, and *ARHGAP24* were first detected in EPs and showed increased activity in LPs (Figure S2K). We surveyed the expression of these disease-associated genes in *in vitro* EP and LP populations, and highlighted podocyte genes that were detected in the *in vitro* derived cells to inform future glomerular disease modeling studies (highlighted in red, Figure S2K).

Vasculature Interactions in Renal Corpuscle Development

Podocytes produce VEGFA, which promotes concurrent development of the vascular network and mesangial support system (Eremina et al., 2003, 2006). Organoids generated via the Morizane protocol adopted here are largely avascular (Figure S4B). To determine whether codevelopment with vascular cell types may normalize podocyte maturation programs, DD 13-14 organoids were implanted beneath the kidney capsule of NOD SCID mice (Figure 5A). Live imaging of blood flow facilitated by plasma labeling showed organoids were well-vascularized by the host mouse circulatory system (Plvap+) 10 days after implantation (Figure 5B and Video S1). *OLFM3* and GFRA3, EP signature genes which display persistent activity *in vitro*, continued to be expressed in late vascularized podocytes post transplantation (Figures 5D and 5F), Similarly, we failed to observed normalization of the LP signature gene *TNNT2,* which remained undetectable in PLCs post transplantation (Figure 5E); however, *COL4A3*, mutations which result in glomerular degeneration in Alport syndrome, was now expressed in vascularized podocytes (Figure 5D). Thus, vascular interactions partially normalized the expression of a critical component of the glomerular basement membrane.

Our scRNA-seq analyses indicate that pericytes and MCs were absent in the avascular organoids (Figure S4B). In vascularized organoids, MAFB+ HuNu+ *in vitro*-derived podocytes formed renal corpuscle-like structure with PDGFRB+ HuNu+ organoid interstitial cells and PECAM1+ HuNu- mouse ECs (HuNu: Human Nucleus) (Figure 5C). Although *TMEFF2* was not detected in PDGFRB+ cells recruited to podocyte clusters (data not showed), expression of GATA3 lends support to human organoid-derived interstitial cells adopting an early pericyte identity (Figure 5J). Additionally, the expression of *GATA5* in mouse ECs attracted to podocyte clusters supports the activation of an early glomerular-specific vascular signature (Figure 5K).

In summary, *in vitro* derived podocytes nucleate vascular (host-derived) and mesangial (graft-derived) developmental programs, suggesting full maturation requires interplay among all of these cell types.

DISCUSSION

In this study, we extended recent reports from our group and others of human fetal kidney development, with a focus on the programs underlying human podocyte development (Lindström et al., 2018d; Menon et al., 2018). These data provide a benchmark for an unbiased assessment of human podocyte development, as well as a resource for mining of regulatory mechanism to improve kidney organoid-directed programing of the kidney's filtration system.

Development of the Human Podocyte

Deep profiling identified transcriptomic changes highlighting temporally distinct gene expression profiles in the staged progression of podocyte maturation. The transition from NPC to EP is associated with the down-regulation of a large set of ribosomal protein-encoding genes that remain active in other cell types of the human fetal kidney (Figures S4I and S4J), and the activation of EP signature genes profiled in our previous studies (Lindström et al., 2018c), several of which are critical for the formation of the mouse kidney (Müller et al., 1997; Ohuchi et al., 2000; Xu et al., 1999, 2003). NPCs are highly proliferative; however, proliferation drops as NPCs commit to EP precursors, which undergo terminal cell divisions prior to forming mitotically quiescent mature podocytes (Hiromura et al., 2001). Genes of group EP2 are expressed transiently in the RV, SSB, and CLSN podocyte precursors, among which the expression of *HEY1, CDH6, PAX8, JAG1, OLFM3*, *PCDH9,* and *LHX1* in human podocyte precursors has been documented (Lindström et al., 2018a, 2018d). Though their specific roles in podocyte development have not been examined, *Cdh6*, *Pax8,* and *Lhx1* have been reported to play important roles in mouse kidney formation or

(G) Volcano plot displaying genes either enriched in human LPs or organoid LPs. Blue text highlighting genes plotted in (H).
(H) Heatmaps showing expression of selected OrgLP-enriched genes (*C11orf71, GFRA3, ITIH5, OLFM3*, and *LEFTY1*) and HuLP-enriched genes (*PLA2R1, COL4A4, TNNT2*, *COL4A3,* and *LOX*) along the *in vivo* or *in vitro* podocyte differentiation trajectory.
(I and J) Feature plots showing expression of *ANXA1* and *GFRA3* analyzed using scRNA-seq of week 17 human fetal kidney (I) or kidney organoids (J).

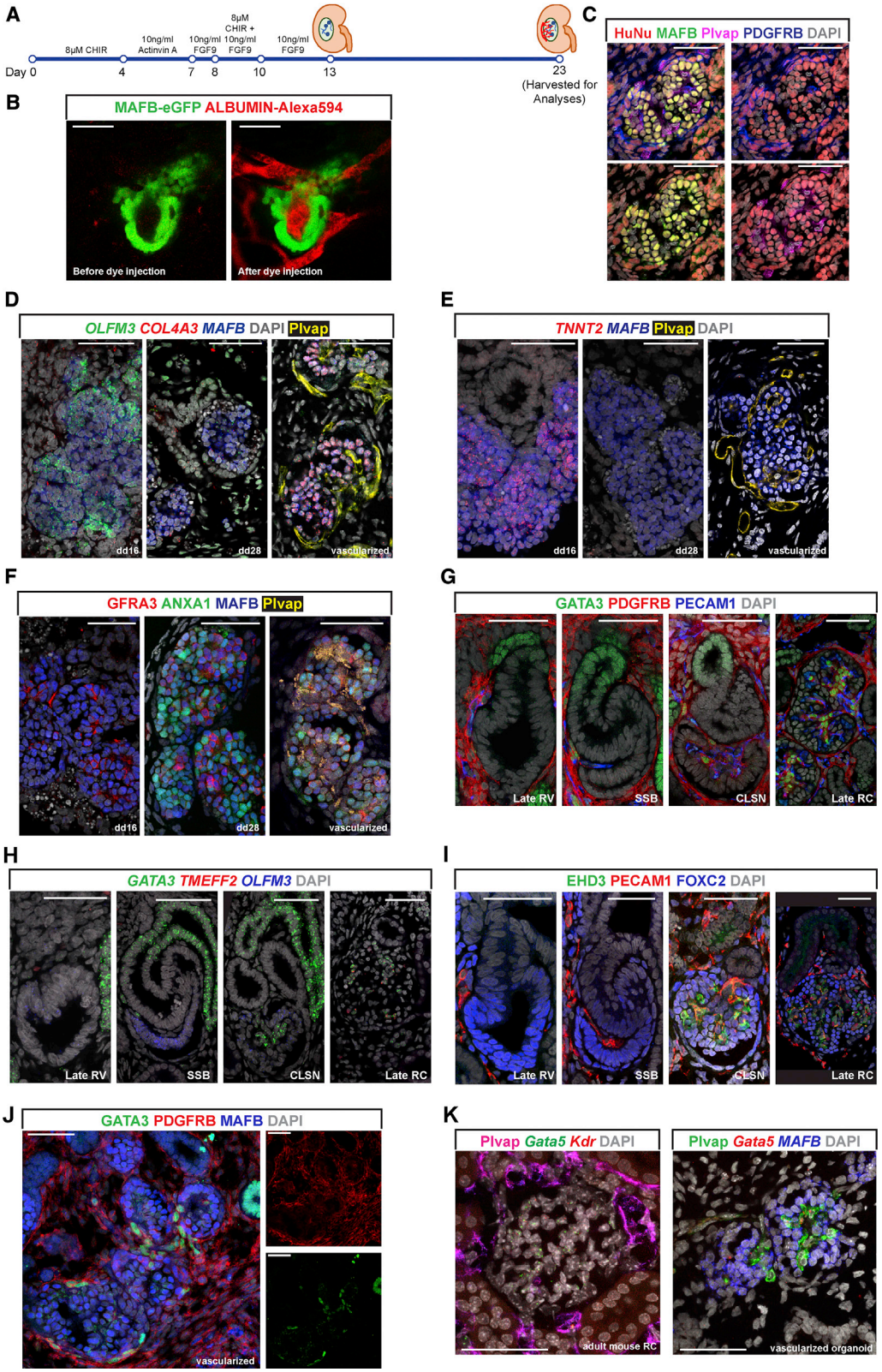

Figure 5. Examination of Vasculature's Contribution to Glomerular Construction

(A) Schematic diagram summarizing the experimental design to vascularize *in vitro* derived podocytes.

(B) Multi-photon imaging snapshots of vascularized *in vitro* derived podocytes before and after Alexa 594-conjugated albumin dye injection. Scale bars: 50 μm.

(legend continued on next page)

nephron induction (Bouchard et al., 2002; Kobayashi et al., 2005; Mah et al., 2000). Group EP3 comprises genes upregulated only in the CLSN, possibly as a transient response to endothelial and mesangial invasion and early establishment of signaling center at slit diaphragm. Among these, the transient expression of *GFRA3*, encoding GDNF receptor α3, hints at the possible importance of GDNF signaling in this specific time window of podocyte and glomerular formation.

Among LP signature genes, group LP1 are detected as early as RV-stage podocyte precursors and maintain expression in LP development, while LP2 genes are highly expressed in late RC podocytes. A large portion of these are disease-relevant ECM protein-encoding genes, some with known functions in mouse podocyte development (including *ACTN4*, *NPHS1*, *NPHS2*, *PODXL*, *SYNPO*, *TJP1, PLCE1, COL4A3,* and *COL4A4*) (Ahvenainen et al., 1956; Asanuma et al., 2006; Boute et al., 2000; Invest, 1970; Itoh et al., 2014; Kaplan et al., 2000; Lepori et al., 2018; Online Mendelian Inheritance in Man, 2018). Our comparative analyses with the mouse podocyte transcriptional profiles highlight novel cross-species shared LP genes. For instance, *PHACTR4* (Phosphatase and Actin Regulator 4) has been shown to regulate directional migration of enteric neural crest cells (Zhang et al., 2012), but its importance in podocyte cytoskeletal architecture and migration has not been studied. Additionally, the anti-inflammatory function of *ANXA1* (Annexin A1) has been highlighted in diseases of various organ systems (Jong et al., 2016; Ries et al., 2016) and may function in podocyte antigen presenting activities (Goldwich et al., 2013). Notably, we also identified novel human LP-specific genes (including *S100A6, MYL9, TPPP6, SNCA, TNNI1, TNNT2, MYL12, PDLIM2, PALLD,* and *GSN*) that are associated with cytoskeletal proteins, suggesting species-specific functions in maintaining podocyte architecture.

Temporal expression of EP and LP genes is likely to be orchestrated by temporal programs of transcription factor activity. *SIX1, SIX2*, *EYA1*, and *MEOX1*, which are linked to the maintenance of mouse and human NPCs (Kobayashi et al., 2008; O'Brien et al., 2016; Self et al., 2006; Xu et al., 1999, 2003), could play a role in EP1 gene activation, while PAX8, LHX1, and HEY1 activity would be more likely to play a role in EP2 and EP3 programs. Clearly, transient EP-restricted activity of these transcription factors rules out a progressive role in specification of mature podocytes. Transcription factors known to play essential roles specifically in podocyte development (e.g. *TCF21* and *MAFB*) were first detected in RV-stage podocyte precursors overlapping with NPC genes (*SIX1* and *TMEM100*). Evidence points to conserved functions for several podocyte-specifying transcriptional regulators between mouse and human, with activity continuing into LP programs regulating podocyte morphogenesis (Maezawa et al., 2014; Moriguchi et al., 2006). Signaling inputs from the slit diaphragm established at the capillary loop stage likely regulate LP gene activity (Greka and Mundel, 2012; Schell et al., 2014).

The renal corpuscle is composed of three tightly interacting cellular components: podocytes, vascular, and MCs. Disrupting their interaction results in defective renal corpuscle development in the mouse kidney (Eremina et al., 2003, 2006; Kikkawa et al., 2003; Levéen et al., 1994; Lindahl et al., 1998; Soriano, 1994). Our analysis is consistent with a conserved role of VEGF signaling in recruitment and organization of the vasculature. A transient activation of *SEMA3A* was observed in EPs; Sema3a regulates morphogenesis of podocytes and recruitment of ECs in the mouse kidney (Reidy et al., 2009). We also observed *FBLN2* expression in podocytes; *Fbln2* is required for vessel wall integrity (Chapman et al., 2010; Xu and Shi, 2014), and recent studies link *Fbln2* to promoting vascular invasion (A.D. K., personal communication).

Development of *In Vitro* Derived Podocytes in Comparison with the *In Vivo* Counterpart and Roles of the Vasculature in Renal Corpuscle Development

Recent studies have employed scRNA-seq technology to identify kidney-like cell types in organoids through common markers (Table 1) (Czerniecki et al., 2018; Hale et al., 2018; Sharmin et al., 2016; Wu et al., 2018a; Yoshimura et al., 2017). Our developmental biology-driven analyses deepen the understanding of the *in vitro* system, highlighting a differentiation trajectory similar to human podocyte development in the fetal kidney. The *in vivo* data will facilitate efforts to improve cell culture-directed methods of podocyte production and the prediction of regulatory mechanisms in the podocyte program. Of note, despite the absence of vascular or mesangial cell types, comparison of *in vitro*-derived MAFB-eGFP+ cells with the *in vivo* podocyte developmental program indicated a striking overlap: 137 of 158 EP genes and 84 of 104 LP genes were expressed as expected. Podocytes in organoid transplants attract and interact with host vasculature and interstitial cells in the vicinity upregulate a pericyte signature. Furthermore, there is a normalization of donor human podocyte programs in transplants. Together, these results suggest that further improvements can be made *in vitro* through the optimization of mesangial and vascular compartments in the organoid models.

Our organoid approach was centered around generating the metanephric component of the kidney (Morizane and Bonventre, 2016; Morizane et al., 2015), and the absence of vascular cells can be due to distinct spatial and temporal developmental origin. Additionally, vascular development is heavily dependent on VEGF and a low physiological oxygen level (Kusuma et al., 2014); current organoid growth conditions may not favor growth

(C) IF analysis of vascularized organoids showing human or mouse origins of podocytes, interstitial, and vascular components. Scale bars: 50 μm.
(D and E) Fluorescent *in situ* hybridization showing expression of EP gene (*OLFM3*) and LP genes (*COL4A3* and *TNNT2*) in DD 16, DD 28 and vascularized *in vitro* derived MAFB+ podocytes. Scale bars: 50 μm.
(F) IF stains of DD 16, DD 28, and vascularized *in vitro* derived podocytes. Scale bars: 50 μm.
(G and H) IF stain (G) and fluorescent *in situ* hybridization (H) highlighting PDGFRB+ GATA3+ pericytes and GATA3+ TMEFF2+ mesangial cells in human developing nephrons. Scale bars: 50 μm.
(I) IF analysis showing EHD3+ PECAM1+ glomerular endothelial cells in human developing nephrons. Scale bars: 50 μm.
(J) IF stain showing expression of GATA3 in interstitial cells recruited to podocyte clusters. Scale bars: 50 μm.
(K) IF stain combined with *in situ* hybridization (italicized gene names) showing mouse *Gata5*+ glomerular vascular cells in adult mouse renal corpuscle (left panel) and vascularized organoid (right panel). Scale bars: 50 μm.

Table 1. Review Recent Approaches to Assess *In Vitro*-Derived Podocytes

Study	Reporter Cell Line for Podocyte Identification	Comparison with *In Vivo* Podocytes		
		In Vivo Sample Type	Method	Findings
Sharmin et al. (2016)	NPHS1-GFP iPSC	mouse adult podocytes, human glomeruli	microarray	shared genes among *in vitro* podocytes, human glomeruli, and mouse adult podocytes are enriched for podocyte signature genes
Wu et al. (2018a)	N/A	adult kidney cells	single-cell RNA-seq of organoids, and single-nucleus RNA-seq of human adult kidney biopsy	identified PLCs in organoids by comparing average gene expression of organoid and human fetal kidney cell clusters
Hale et al., 2018	MAFB-BFP iPSC	human matrisome database	mass spectrometry	*in vitro* 3D-cultured podocytes and human matrisome have shared extracellular matrix proteins
Czerniecki et al. (2018)	N/A	human fetal kidney (Menon et al., 2018)	single-cell RNA-seq of organoids and human fetal kidney	identified PLCs in organoids by comparing average gene expression of organoid and human fetal kidney cell clusters
Combes et al., 2019	N/A	human fetal kidney (Lindström et al., 2018d)	single-cell RNA-seq of organoids and human fetal kidney	identified PLCs in organoids by comparing average gene expression of organoid and human fetal kidney cell clusters
Yoshimura et al., 2019	NPHS1-GFP iPSC	human adult podocytes	RNA-seq	identified shared and different gene expression profiles between *in vitro* and *in vivo* podocytes
this study	MAFB-eGFP H9 hESC	human fetal kidney	single-cell RNA-seq of organoids and human fetal kidney	identifed shared transcriptional signatures between *in vitro* and *in vivo* podocyte development, pinpointed abnormal gene expression *in vitro*, and highlighted the potential of *in vitro*-derived podocytes as a model for human podocyte development and disease studies

of low numbers of vascular cells. Recently, Czerniecki and colleagues described an approach to generate kidney organoids with ECs (Czerniecki et al., 2018). Our studies can facilitate assessment of glomerular endothelial specification as well as effects of ECs on podocyte maturation and mesangial cell commitment *in vitro*. Interestingly, flow in bioengineered kidney organoid chips enhances endothelial growth though the effects on the maturation of renal corpuscle cell types is not clear (Homan et al., 2019). Predictions of ligand-receptor interactions among the RC cell types may help with these efforts (Table S2).

STAR★METHODS

Detailed methods are provided in the online version of this paper and include the following:

- KEY RESOURCES TABLE
- LEAD CONTACT AND MATERIALS AVAILABILITY
- EXPERIMENTAL MODEL AND SUBJECT DETAILS
  - Human Kidney Studies
  - Human Embryonic Stem Cell Line (hESC)
- METHOD DETAILS
  - hESC Maintenance and Differentiation to Generate Kidney Organoids
  - Immunofluorescent Analyses
  - *In Situ* Hybridization
  - Single-Cell RNA-Sequencing and Analyses of Human Fetal Kidneys
  - Single-Cell RNA-Sequencing and Analyses of Human Kidney Organoids
  - Pseudotime Reconstruction of Lineages
  - Differentially Expressed Gene Test between Two Podocyte Clusters
  - EP and LP Gene List Generation
  - Receptor-Ligand Analysis
  - Hierarchical Clustering of Human Week 17 Clusters and Organoid Cell Clusters
  - SWNE Analysis of the Merged Human Week 17 and Organoid Cell Clusters
  - mRNA-Seq of MAFB-eGFP+ Cells from Kidney Organoids
  - mRNA-Seq of Human Fetal Renal Corpuscles
  - mRNA-Seq of Immortalized Podocytes
  - mRNA-Seq Data Analysis
  - Gene-List GO-Term Queries
  - Glomerular Disease-Related Gene Expression Analysis
  - Analysis of Published scRNASeq Dataset
  - Analysis of Microarray Datasets
  - Renal Capsule Transplant
  - Intravital Multiphoton Microscopy
- DATA AND CODE AVAILABILITY

SUPPLEMENTAL INFORMATION

Supplemental Information can be found online at https://doi.org/10.1016/j.devcel.2019.06.001.

ACKNOWLEDGMENTS

We thank the McMahon Lab members for insightful discussions. Work in A.P.M.'s laboratory was supported by grants from the NIH (DK054364 and DK110792).

AUTHOR CONTRIBUTIONS

T.T., N.O.L., and A.P.M. planned experiments and analyzed data; T.T. assembled the figures; T.T., N.O.L., A.R., G.D.S.B., Q.G., A.D.K., B.D., J.A.M. collected data; M.T. and B.G. provided embryonic and fetal kidneys; J.P.P. supervised intravital multi-photon imaging; J.M. managed resources needed for experiments, T.T., N.O.L., and A.P.M. wrote the manuscript incorporating input from all authors.

DECLARATION OF INTERESTS

The authors declare no competing interests.

Received: December 17, 2018
Revised: March 27, 2019
Accepted: May 31, 2019
Published: July 1, 2019

REFERENCES

Ahvenainen, E.K., Hallman, N., and Hjelt, L. (1956). Nephrotic syndrome in newborn and young infants. Ann. Paediatr. Fenn. *2*, 227–241.

Asanuma, K., Yanagida-Asanuma, E., Faul, C., Tomino, Y., Kim, K., and Mundel, P. (2006). Synaptopodin orchestrates actin organization and cell motility via regulation of RhoA signalling. Nat. Cell Biol. *8*, 485–491.

Bantounas, I., Ranjzad, P., Tengku, F., Silajdžić, E., Forster, D., Asselin, M.-C.C., Lewis, P., Lennon, R., Plagge, A., Wang, Q., et al. (2018). Generation of functioning nephrons by implanting human pluripotent stem cell-derived kidney progenitors. Stem Cell Reports *10*, 766–779.

Berry, R.L., Ozdemir, D.D., Aronow, B., Lindström, N.O., Dudnakova, T., Thornburn, A., Perry, P., Baldock, R., Armit, C., Joshi, A., et al. (2015). Deducing the stage of origin of Wilms' tumours from a developmental series of Wt1-mutant mice. Dis. Model Mech. *8*, 903–917.

Bouchard, M., Souabni, A., Mandler, M., Neubüser, A., and Busslinger, M. (2002). Nephric lineage specification by Pax2 and Pax8. Genes Dev. *16*, 2958–2970.

Boute, N., Gribouval, O., Roselli, S., Benessy, F., Lee, H., Fuchshuber, A., Dahan, K., Gubler, M.C., Niaudet, P., and Antignac, C. (2000). NPHS2, encoding the glomerular protein podocin, is mutated in autosomal recessive steroid-resistant nephrotic syndrome. Nat. Genet. *24*, 349–354.

Brunskill, E.W., Georgas, K., Rumballe, B., Little, M.H., and Potter, S.S. (2011). Defining the molecular character of the developing and adult kidney podocyte. PLoS One *6*, e24640.

Carvalho, B.S., and Irizarry, R.A. (2010). A framework for oligonucleotide microarray preprocessing. Bioinformatics *26*, 2363–2367.

Chapman, S.L., Sicot, F.X., Davis, E.C., Huang, J., Sasaki, T., Chu, M.L., and Yanagisawa, H. (2010). Fibulin-2 and Fibulin-5 cooperatively function to form the internal elastic lamina and protect From vascular injury. Arterioscler. Thromb. Vasc. Biol. *30*, 68–74.

Chau, Y.Y., Brownstein, D., Mjoseng, H., Lee, W.C., Buza-Vidas, N., Nerlov, C., Jacobsen, S.E., Perry, P., Berry, R., Thornburn, A., et al. (2011). Acute multiple organ failure in adult mice deleted for the developmental regulator Wt1. PLoS Genet. *7*, e1002404.

Chen, J., Bardes, E.E., Aronow, B.J., and Jegga, A.G. (2009). ToppGene Suite for gene list enrichment analysis and candidate gene prioritization. Nucleic Acids Res. *37*, W305–W311.

Chung, N.C., and Storey, J.D. (2015). Statistical significance of variables driving systematic variation in high-dimensional data. Bioinformatics *31*, 545–554.

Combes, A., Zappia, L., Er, P., Oshlack, A., and Little, M. (2019). Single-cell analysis reveals congruence between kidney organoids and human fetal kidney. Genome Med *11*, 3.

Czerniecki, S.M., Cruz, N.M., Harder, J.L., Menon, R., Annis, J., Otto, E.A., Gulieva, R.E., Islas, L.V., Kim, Y.K., Tran, L.M., et al. (2018). High-throughput screening enhances kidney organoid differentiation from human pluripotent stem cells and enables automated multidimensional phenotyping. Cell Stem Cell *22*, 929–940.

Eremina, V., Cui, S., Gerber, H., Ferrara, N., Haigh, J., Nagy, A., Ema, M., Rossant, J., Jothy, S., Miner, J.H., et al. (2006). Vascular endothelial growth factor A signaling in the podocyte-endothelial compartment is required for mesangial cell migration and survival. J. Am. Soc. Nephrol. *17*, 724–735.

Eremina, V., Sood, M., Haigh, J., Nagy, A., Lajoie, G., Ferrara, N., Gerber, H.P., Kikkawa, Y., Miner, J.H., and Quaggin, S.E. (2003). Glomerular-specific alterations of VEGF-A expression lead to distinct congenital and acquired renal diseases. J. Clin. Invest. *111*, 707–716.

Freedman, B.S., Brooks, C.R., Lam, A.Q., Fu, H., Morizane, R., Agrawal, V., Saad, A.F., Li, M.K., Hughes, M.R., Werff, R.V., et al. (2015). Modelling kidney disease with CRISPR-mutant kidney organoids derived from human pluripotent epiblast spheroids. Nat. Commun. *6*, 8715.

Gebeshuber, C.A., Kornauth, C., Dong, L., Sierig, R., Seibler, J., Reiss, M., Tauber, S., Bilban, M., Wang, S., Kain, R., et al. (2013). Focal segmental glomerulosclerosis is induced by microRNA-193a and its downregulation of WT1. Nat. Med. *19*, 481–487.

Goldwich, A., Burkard, M., Ölke, M., Daniel, C., Amann, K., Hugo, C., Kurts, C., Steinkasserer, A., and Gessner, A. (2013). Podocytes are nonhematopoietic professional antigen-presenting cells. J. Am. Soc. Nephrol. *24*, 906–916.

Greka, A., and Mundel, P. (2012). Cell biology and pathology of podocytes. Annu. Rev. Physiol. *74*, 299–323.

Hackl, M.J., Burford, J.L., Villanueva, K., Lam, L., Suszták, K., Schermer, B., Benzing, T., and Peti-Peterdi, J. (2013). Tracking the fate of glomerular epithelial cells in vivo using serial multiphoton imaging in new mouse models with fluorescent lineage tags. Nat. Med. *19*, 1661–1666.

Hale, L.J., Howden, S.E., Phipson, B., Lonsdale, A., Er, P.X., Ghobrial, I., Hosawi, S., Wilson, S., Lawlor, K.T., Khan, S., et al. (2018). 3D organoid-derived human glomeruli for personalised podocyte disease modelling and drug screening. Nat Commun *9*, 5167.

Hammes, A., Guo, J.K., Lutsch, G., Leheste, J.R., Landrock, D., Ziegler, U., Gubler, M.C., and Schedl, A. (2001). Two splice variants of the Wilms' tumor 1 gene have distinct functions during sex determination and nephron formation. Cell *106*, 319–329.

Hiromura, K., Haseley, L.A., Zhang, P., Monkawa, T., Durvasula, R., Petermann, A.T., Alpers, C.E., Mundel, P., and Shankland, S.J. (2001). Podocyte expression of the CDK-inhibitor p57 during development and disease. Kidney Int. *60*, 2235–2246.

Homan, K.A., Gupta, N., Kroll, K.T., Kolesky, D.B., Skylar-Scott, M., Miyoshi, T., Mau, D., Valerius, M.T., Ferrante, T., Bonventre, J.V., et al. (2019). Flow-enhanced vascularization and maturation of kidney organoids in vitro. Nat. Methods *16*, 255–262.

Invest, M.-A. (1970). Glomerular polyanion. Alteration in aminoucleoside nephrosis. Lab. Invest.

Itoh, M., Nakadate, K., Horibata, Y., Matsusaka, T., Xu, J., Hunziker, W., and Sugimoto, H. (2014). The structural and functional organization of the podocyte filtration slits is regulated by Tjp1/ZO-1. PLoS One *9*, e106621.

Jong, R., Leoni, G., Drechsler, M., and Soehnlein, O. (2016). The advantageous role of annexin A1 in cardiovascular disease. Cell Adh. Migr. *11*, 261–274.

Kang, J.J., Toma, I., Sipos, A., McCulloch, F., and Peti-Peterdi, J. (2006). Quantitative imaging of basic functions in renal (patho)physiology. Am. J. Physiol. Renal Physiol. *291*, F495–F502.

Kann, M., Ettou, S., Jung, Y.L., Lenz, M.O., Taglienti, M.E., Park, P.J., Schermer, B., Benzing, T., and Kreidberg, J.A. (2015). Genome-wide analysis of Wilms' tumor 1-controlled gene expression in podocytes reveals key regulatory mechanisms. J. Am. Soc. Nephrol. *26*, 2097–2104.

Kaplan, J.M., Kim, S.H., North, K.N., Rennke, H., Correia, L.A., Tong, H.Q., Mathis, B.J., Rodríguez-Pérez, J.C., Allen, P.G., Beggs, A.H., et al. (2000). Mutations in ACTN4, encoding alpha-actinin-4, cause familial focal segmental glomerulosclerosis. Nat. Genet. *24*, 251–256.

Kikkawa, Y., Virtanen, I., and Miner, J.H. (2003). Mesangial cells organize the glomerular capillaries by adhering to the G domain of laminin alpha5 in the glomerular basement membrane. J. Cell Biol. *161*, 187–196.

Kim, D., Pertea, G., Trapnell, C., Pimentel, H., Kelley, R., and Salzberg, S.L. (2013). TopHat2: accurate alignment of transcriptomes in the presence of insertions, deletions and gene fusions. Genome Biol. *14*, R36.

Kim, Y.K., Refaeli, I., Brooks, C.R., Jing, P., Gulieva, R.E., Hughes, M.R., Cruz, N.M., Liu, Y., Churchill, A.J., Wang, Y., et al. (2017). Gene-edited human kidney organoids reveal mechanisms of disease in podocyte development. Stem Cells *35*, 2366–2378.

Kobayashi, A., Kwan, K.M., Carroll, T.J., McMahon, A.P., Mendelsohn, C.L., and Behringer, R.R. (2005). Distinct and sequential tissue-specific activities of the LIM-class homeobox gene Lim1 for tubular morphogenesis during kidney development. Development *132*, 2809–2823.

Kobayashi, A., Valerius, M.T., Mugford, J.W., Carroll, T.J., Self, M., Oliver, G., and McMahon, A.P. (2008). Six2 defines and regulates a multipotent self-renewing nephron progenitor population throughout mammalian kidney development. Cell Stem Cell *3*, 169–181.

Kusuma, S., Peijnenburg, E., Patel, P., and Gerecht, S. (2014). Low oxygen tension enhances endothelial fate of human pluripotent stem cells. Arterioscler. Thromb. Vasc. Biol. *34*, 913–920.

Lee, J.W., Chou, C.-L.L., and Knepper, M.A. (2015). Deep sequencing in microdissected renal tubules identifies nephron segment-specific transcriptomes. J. Am. Soc. Nephrol. *26*, 2669–2677.

Lepori, N., Zand, L., Sethi, S., Fernandez-Juarez, G., and Fervenza, F.C. (2018). Clinical and pathological phenotype of genetic causes of focal segmental glomerulosclerosis in adults. Clin. Kidney J. *11*, 179–190.

Levéen, P., Pekny, M., Gebre-Medhin, S., Swolin, B., Larsson, E., and Betsholtz, C. (1994). Mice deficient for PDGF B show renal, cardiovascular, and hematological abnormalities. Genes Dev. *8*, 1875–1887.

Lindahl, P., Hellström, M., Kalén, M., Karlsson, L., Pekny, M., Pekna, M., Soriano, P., and Betsholtz, C. (1998). Paracrine PDGF-B/PDGF-Rbeta signaling controls mesangial cell development in kidney glomeruli. Development *125*, 3313–3322.

Lindström, N.O., Tran, T., Guo, J., Rutledge, E., Parvez, R.K., Thornton, M.E., Grubbs, B., McMahon, J.A., and McMahon, A.P. (2018a). Conserved and divergent molecular and anatomic features of human and mouse nephron patterning. J. Am. Soc. Nephrol *29*, 825–840.

Lindström, N.O., McMahon, J.A., Guo, J., Tran, T., Guo, Q., Rutledge, E., Parvez, R.K., Saribekyan, G., Schuler, R.E., Liao, C., et al. (2018b). Conserved and divergent features of human and mouse kidney organogenesis. J. Am. Soc. Nephrol. *29*, 785–805.

Lindström, N.O., Guo, J., Kim, A.D., Tran, T., Guo, Q., De Sena Brandine, G., Ransick, A., Parvez, R.K., Thornton, M.E., Baskin, L., et al. (2018c). Conserved and divergent features of mesenchymal progenitor cell types within the cortical nephrogenic niche of the human and mouse kidney. J. Am. Soc. Nephrol. *29*, 806–824.

Lindström, N.O., De Sena Brandine, G., Tran, T., Ransick, A., Suh, G., Guo, J., Kim, A.D., Parvez, R.K., Ruffins, S.W., Rutledge, E.A., et al. (2018d). Progressive recruitment of mesenchymal progenitors reveals a time-dependent process of cell fate acquisition in mouse and human nephrogenesis. Dev. Cell *45*, 651–660.

Love, M.I., Huber, W., and Anders, S. (2014). Moderated estimation of fold change and dispersion for RNA-seq data with DESeq2. Genome Biol. *15*, 550.

Maezawa, Y., Onay, T., Scott, R.P., Keir, L.S., Dimke, H., Li, C., Eremina, V., Maezawa, Y., Jeansson, M., Shan, J., et al. (2014). Loss of the podocyte-expressed transcription factor Tcf21/Pod1 results in podocyte differentiation defects and FSGS. J. Am. Soc. Nephrol. *25*, 2459–2470.

Mah, S.P., Saueressig, H., Goulding, M., Kintner, C., and Dressler, G.R. (2000). Kidney development in Cadherin-6 mutants: delayed mesenchyme-to-epithelial conversion and loss of nephrons. Dev. Biol. *223*, 38–53.

McMahon, A.P. (2016). Development of the mammalian kidney. Curr. Top. Dev. Biol. *117*, 31–64.

Menon, R., Otto, E.A., Kokoruda, A., Zhou, J., Zhang, Z., Yoon, E., Chen, Y.-C.C., Troyanskaya, O., Spence, J.R., Kretzler, M., et al. (2018). Single-cell analysis of progenitor cell dynamics and lineage specification in the human fetal kidney. Development *145*.

Messaoudi, S., He, Y., Gutsol, A., Wight, A., Hébert, R.L., Vilmundarson, R.O., Makrigiannis, A.P., Chalmers, J., Hamet, P., Tremblay, J., et al. (2015). Endothelial Gata5 transcription factor regulates blood pressure. Nat. Commun. *6*, 8835.

Moore, A.W., McInnes, L., Kreidberg, J., Hastie, N.D., and Schedl, A. (1999). YAC complementation shows a requirement for Wt1 in the development of epicardium, adrenal gland and throughout nephrogenesis. Development *126*, 1845–1857.

Moriguchi, T., Hamada, M., Morito, N., Terunuma, T., Hasegawa, K., Zhang, C., Yokomizo, T., Esaki, R., Kuroda, E., Yoh, K., et al. (2006). MafB is essential for renal development and F4/80 expression in macrophages. Mol. Cell. Biol. *26*, 5715–5727.

Morizane, R., and Bonventre, J. (2016). Generation of nephron progenitor cells and kidney organoids from human pluripotent stem cells. Nat Protoc *12*, 195–207.

Morizane, R., Lam, A.Q., Freedman, B.S., Kishi, S., Valerius, M.T., and Bonventre, J.V. (2015). Nephron organoids derived from human pluripotent stem cells model kidney development and injury. Nat. Biotechnol. *33*, 1193–1200.

Müller, U., Wang, D., Denda, S., Meneses, J.J., Pedersen, R.A., and Reichardt, L.F. (1997). Integrin alpha8beta1 is critically important for epithelial-mesenchymal interactions during kidney morphogenesis. Cell *88*, 603–613.

Ni, L., Saleem, M., and Mathieson, P.W. (2012). Podocyte culture: tricks of the trade. Nephrology *17*, 525–531.

O'Brien, L.L., Guo, Q., Lee, Y., Tran, T., Benazet, J.D., Whitney, P.H., Valouev, A., and McMahon, A.P. (2016). Differential regulation of mouse and human nephron progenitors by the six family of transcriptional regulators. Development *143*, 595–608.

O'Rahilly, R., and Müller, F. (2010). Developmental stages in human embryos: revised and new measurements. Cells Tissues Organs *192*, 73–84.

O'Rahilly, R., Müller, F., Hutchins, G.M., and Moore, G.W. (1987). Computer ranking of the sequence of appearance of 73 features of the brain and related structures in staged human embryos during the sixth week of development. Am. J. Anat. *180*, 69–86.

Ohuchi, H., Hori, Y., Yamasaki, M., Harada, H., Sekine, K., Kato, S., and Itoh, N. (2000). FGF10 acts as a major ligand for FGF Receptor 2 IIIb in mouse multi-organ development. Biochem. Biophys. Res. Commun. *277*, 643–649.

Online Mendelian Inheritance in Man. (2018). OMIM® (McKusick-Nathans Institute of Genetic Medicine, Johns Hopkins University). https://omim.org.

Qiu, X., Mao, Q., Tang, Y., Wang, L., Chawla, R., Pliner, H.A., and Trapnell, C. (2017). Reversed graph embedding resolves complex single-cell trajectories. Nat. Methods *14*, 979–982.

Ramilowski, J.A., Goldberg, T., Harshbarger, J., Kloppmann, E., Lizio, M., Satagopam, V.P., Itoh, M., Kawaji, H., Carninci, P., Rost, B., et al. (2015). A draft network of ligand-receptor-mediated multicellular signalling in human. Nat. Commun. *6*, 7866.

Reidy, K.J., Villegas, G., Teichman, J., Veron, D., Shen, W., Jimenez, J., Thomas, D., and Tufro, A. (2009). Semaphorin3a regulates endothelial cell

number and podocyte differentiation during glomerular development. Development *136*, 3979–3989.

Ries, M., Loiola, R., Shah, U.N., Gentleman, S.M., Solito, E., and Sastre, M. (2016). The anti-inflammatory annexin A1 induces the clearance and degradation of the amyloid-β peptide. J. Neuroinflamm. *13*, 234.

Ritchie, M.E., Phipson, B., Wu, D., Hu, Y., Law, C.W., Shi, W., and Smyth, G.K. (2015). limma powers differential expression analyses for RNA-sequencing and microarray studies. Nucleic Acids Res. *43*, e47.

Sadl, V., Jin, F., Yu, J., Cui, S., Holmyard, D., Quaggin, S., Barsh, G., and Cordes, S. (2002). The mouse Kreisler (Krml1/MafB) segmentation gene is required for differentiation of glomerular visceral epithelial cells. Dev Biol *249*, 16–29.

Saleem, M.A., O'Hare, M.J., Reiser, J., Coward, R.J., Inward, C.D., Farren, T., Xing, C.Y., Ni, L., Mathieson, P.W., and Mundel, P. (2002). A conditionally immortalized human podocyte cell line demonstrating nephrin and podocin expression. J. Am. Soc. Nephrol. *13*, 630–638.

Satija, R., Farrell, J.A., Gennert, D., Schier, A.F., and Regev, A. (2015). Spatial reconstruction of single-cell gene expression data. Nat. Biotechnol. *33*, 495–502.

Schell, C., Wanner, N., and Huber, T.B. (2014). Glomerular development – shaping the multi-cellular filtration unit. Semin. Cell Dev. Biol. *36*, 39–49.

Scrucca, L., Fop, M., Murphy, T.B., and Raftery, A.E. (2016). Mclust 5: clustering, classification and density estimation using Gaussian finite mixture models. R J. *8*, 289–317.

Self, M., Lagutin, O.V., Bowling, B., Hendrix, J., Cai, Y., Dressler, G.R., and Oliver, G. (2006). Six2 is required for suppression of nephrogenesis and progenitor renewal in the developing kidney. EMBO J. *25*, 5214–5228.

Sharmin, S., Taguchi, A., Kaku, Y., Yoshimura, Y., Ohmori, T., Sakuma, T., Mukoyama, M., Yamamoto, T., Kurihara, H., and Nishinakamura, R. (2016). Human induced pluripotent stem cell–derived podocytes mature into vascularized glomeruli upon experimental transplantation. J. Am. Soc. Nephrol. *27*, 1778–1791.

Soriano, P. (1994). Abnormal kidney development and hematological disorders in PDGF beta-receptor mutant mice. Genes Dev. *8*, 1888–1896.

Strachan, T., Lindsay, S., and Wilson, D.I. (1997). Molecular Genetics of Early Human Development (Herndon, VA: BIOS Scientific Publishers, Oxford).

Taguchi, A., Kaku, Y., Ohmori, T., Sharmin, S., Ogawa, M., Sasaki, H., and Nishinakamura, R. (2014). Redefining the in vivo origin of metanephric nephron progenitors enables generation of complex kidney structures from pluripotent stem cells. Cell Stem Cell *14*, 53–67.

Takasato, M., Er, P., Chiu, H., Maier, B., Baillie, G., Ferguson, C., Parton, R., Wolvetang, E., Roost, M., Lopes, S., et al. (2016). Kidney organoids from human iPS cells contain multiple lineages and model human nephrogenesis. Nature *536*, 564–568.

Takasato, M., Er, P.X., Becroft, M., Vanslambrouck, J.M., Stanley, E.G., Elefanty, A.G., and Little, M.H. (2014). Directing human embryonic stem cell differentiation towards a renal lineage generates a self-organizing kidney. Nat. Cell Biol. *16*, 118–126.

Takasato, M., Er, P.X., Chiu, H.S., Maier, B., Baillie, G.J., Ferguson, C., Parton, R.G., Wolvetang, E.J., Roost, M.S., Chuva de Sousa Lopes, S.M., et al. (2015). Kidney organoids from human iPS cells contain multiple lineages and model human nephrogenesis. Nature *526*, 564–568.

Trapnell, C., Pachter, L., and Salsberg, S.L. (2009). TopHat: discovering splice junctions with RNA-seq. Bioinformatics *25*, 1105–1111.

Uhlén, M., Fagerberg, L., Hallström, B.M.M., Lindskog, C., Oksvold, P., Mardinoglu, A., Sivertsson, Å., Kampf, C., Sjöstedt, E., Asplund, A., et al. (2015). Proteomics. tissue-based map of the human proteome. Science *347*, 1260419.

Uhlen, M., Oksvold, P., Fagerberg, L., Lundberg, E., Jonasson, K., Forsberg, M., Zwahlen, M., Kampf, C., Wester, K., Hober, S., et al. (2010). Towards a knowledge-based Human Protein Atlas. Nat. Biotechnol. *28*, 1248–1250.

Van den Berg, C.W., Ritsma, L., Avramut, M.C., Wiersma, L.E., van den Berg, B.M., Leuning, D.G., Lievers, E., Koning, M., Vanslambrouck, J.M., Koster, A.J., et al. (2018). Renal subcapsular transplantation of PSC-derived kidney organoids induces neo-vasculogenesis and significant glomerular and tubular maturation in vivo. Stem Cell Reports *10*, 751–765.

Wu, H., Uchimura, K., Donnelly, E.L., Kirita, Y., Morris, S.A., and Humphreys, B.D. (2018a). Comparative analysis and refinement of human PSC-derived kidney organoid differentiation with single-cell transcriptomics. Cell Stem Cell *23*, 869–881.

Wu, Y., Tamayo, P., and Zhang, K. (2018b). Visualizing and interpreting single-cell gene expression datasets with similarity weighted nonnegative embedding. Cell Syst. *7*, 656–666.

Xu, J., and Shi, G.-P.P. (2014). Vascular wall extracellular matrix proteins and vascular diseases. Biochim. Biophys. Acta *1842*, 2106–2119.

Xu, P.X., Adams, J., Peters, H., Brown, M.C., Heaney, S., and Maas, R. (1999). Eya1-deficient mice lack ears and kidneys and show abnormal apoptosis of organ primordia. Nat. Genet. *23*, 113–117.

Xu, P.X., Zheng, W., Huang, L., Maire, P., Laclef, C., and Silvius, D. (2003). Six1 is required for the early organogenesis of mammalian kidney. Development *130*, 3085–3094.

Yamaguchi, S., Morizane, R., Homma, K., Monkawa, T., Suzuki, S., Fujii, S., Koda, M., Hiratsuka, K., Yamashita, M., Yoshida, T., et al. (2016). Generation of kidney tubular organoids from human pluripotent stem cells. Sci. Rep. *6*, 38353.

Yoshimura, Y., Taguchi, A., and Nishinakamura, R. (2017). Generation of a three-dimensional kidney structure from pluripotent stem cells. Methods Mol. Biol. *1597*, 179–193.

Yoshimura, Y., Taguchi, A., Tanigawa, S., Yatsuda, J., Kamba, T., Takahashi, S., Kurihara, H., Mukoyama, M., and Nishinakamura, R. (2019). Manipulation of nephron-patterning signals enables selective induction of podocytes from human pluripotent stem cells. J Am Soc Nephrol *30*, 304–321.

Zhang, Y., Kim, T.H., and Niswander, L. (2012). Phactr4 regulates directional migration of enteric neural crest through PP1, integrin signaling, and cofilin activity. Genes Dev. *26*, 69–81.

STAR★METHODS

KEY RESOURCES TABLE

REAGENT or RESOURCE	SOURCE	IDENTIFIER
Antibodies		
LHX1	R&D	MAB2725, RRID:AB_2135636
MAFB	R&D	MAB3810, RRID:AB_2137675
PAX8	Abcam	ab189249,
KRT8/18	DSHB	Troma-1
NPHS2	abcam	ab50339, RRID:AB_882097
SYNPO	R&D	MAB8977
TGFBR3	R&D	AF-242-PB, RRID:AB_354417
ANXA1	Cell Signaling	32934
ARMH4/C14orf37	Sigma Aldrich	HPA001789, RRID:AB_1078328
WT1	abcam	ab89901, RRID:AB_2043201
CUBN	Santa Cruz	sc-20607, RRID:AB_2230037
CDH1	Biosciences	610182, RRID:AB_397581
PDGFRB	Abcam	ab32570, RRID:AB_777165
VEGFR2	Cell Signaling	2479, RRID:AB_2212507
GFRA3	R&D	AF670, RRID:AB_2110447
PAX2	R&D	AF3364, RRID:AB_10889828
F3	R&D	AF2339, RRID:AB_442150)
Plvap	BioRad	MCA2539GA, RRID:AB_931734
GATA3	R&D	AF2605, RRID:AB_2108571
PECAM1	BD Pharmingen	BDB550274
EHD3	Novus Biologicals	NBP2-31896
FOXC2	R&D	AF6989, RRID:AB_10973139
Fluorescent *in situ* hybridization probes		
MAFB	Advanced Cell Diagnostics, Inc.	400801-C2
RPS21	Advanced Cell Diagnostics, Inc.	511381-C3
OLFM3	Advanced Cell Diagnostics, Inc.	549051-C3
PLA2R1	Advanced Cell Diagnostics, Inc.	524581
TNNT2	Advanced Cell Diagnostics, Inc.	518991-C3
COL4A3	Advanced Cell Diagnostics, Inc.	461861
Chemicals, Peptides, and Recombinant Proteins		
CHIR99021	Sigma Aldrich	SML1046-25MG
Recombinant Human/Mouse/Rat Activin A Protein	R&D	338-AC-050
Recombinant Human FGF-basic (154 a.a.)	PeproTech	10771–940
Recombinant Human FGF-9 Protein	R&D	273-F9
Recombinant Human VEGF 165 Protein	R&D	293-VE-010
StemFit Basic02	Ajinomoto	Basic02
Y27632	StemCell Technologies	72302
Accutase	StemCell Technologies	07920
Cas9 Protein with NLS	PNA Bio	CP02
mTeSR	StemCell Technologies	85850
Critical Commercial Assays		
Chromium Single Cell 3′ Library & Gel Bead Kit v2	10× Genomics	120237
Chromium Single Cell A Chip Kit	10× Genomics	120236
Chromium i7 Multiplex Kit	10× Genomics	120262

(*Continued on next page*)

Continued		
REAGENT or RESOURCE	SOURCE	IDENTIFIER
RNeasy	QIAGEN	74104
RNAscope® Multiplex Fluorescent Reagent Kit v2	Advanced Cell Diagnostics, Inc.	323100
KAPA Stranded mRNA-Seq Kit	Kapa Biosystems	KK8420
Deposited Data		
Bulk RNA-Seq of human fetal renal corpuscles and whole kidney (minus renal corpuscles)	Gene Expression Omnibus	GSE127344
Bulk RNA-Seq of organoids collected at various differentiation timepoints	Gene Expression Omnibus	GSE124392
scRNA-Seq of human fetal kidneys and organoids (day 16 and day 28)	Gene Expression Omnibus	GSE124472
Experimental Models: Cell Lines		
H9 hESC	WiCell	WA09
Experimental Models: Organisms/Strains		
Immunocompromised mice	The Jackson Laboratory	NOD.CB17-Prkdc<SCID>/J, RRID:MGI:5652139
Software and Algorithms		
Seurat	Satija et al., (2015)	http://satijalab.org/seurat/
Similarity Weighted Nonnegative Embedding (SWNE)	Wu et al., (2018a, 2018b)	https://github.com/yanwu2014/swne
Monocle 2.0	Qiu et al., (2017)	http://cole-trapnell-lab.github.io/monocle-release/
Cell Ranger 2.1	10× Genomics	https://support.10xgenomics.com/single-cell-gene-expression/software/downloads/latest

LEAD CONTACT AND MATERIALS AVAILABILITY

Further information and requests for resources and reagents should be directed to and will be fulfilled by the Lead Contact, Andrew P. McMahon (amcmahon@med.usc.edu).

EXPERIMENTAL MODEL AND SUBJECT DETAILS

Human Kidney Studies

De-identified human fetal tissue was obtained from elective terminations with informed consent with the approval of Institutional Review Boards of both Children's Hospital of Los Angeles and the Keck School of Medicine of the University of Southern California. Gestational age was determined using guidelines from the American College of Obstetricians and Gynecologists using a combination of ultrasound and last menstrual measurements (O'Rahilly and Müller, 2010; O'Rahilly et al., 1987; Strachan et al., 1997). Samples were delivered on ice at 4°C in high glucose DMEM (Gibco) supplemented with 10% fetal bovine serum (Sigma Aldrich) and 25mM HEPES (Gibco).

Human Embryonic Stem Cell Line (hESC)

H9 hESC line (female) was obtained from WiCell (WA09). The MAFB-P2A-eGFP hESC line was generated by knocking-in the P2A-eGFP cassette into the 3' end of *MAFB* locus by employing CRISPR-Cas9 technology. The donor plasmid, gRNA and Cas9 protein were introduced into H9 cells via electroporation (Thermofisher, MPK5000S). For single-cell cloning, the targeted H9 cells were dissociated into single cells using Accutase (StemCell Technologies), and 200 cells were seeded in a Geltrex-coated 100-mm dish with 10ml of mTeSR (supplemented with 10μm Y27632). Single cell-derived colonies were picked up and expanded for Southern blot validations. Key sequences important for cell line generation are listed in Table S2 under "DNA Sequences (cell line)".

METHOD DETAILS

hESC Maintenance and Differentiation to Generate Kidney Organoids

MAFB-P2A-eGFP H9 hESC cells were cultured in StemFit media (Ajinomoto, ASB01-R) supplemented with 10ng/ml of FGF2 (R&D, 273-F9) on Geltrex-coated plates (Geltrex from ThermoFisher, A1413302). When cells reach 60% confluent, differentiation was started following the Bonventre protocol with minor modification: 4 days of 8μM CHIR99021 (Sigma Aldrich, SML1046) treatment, followed by 3 days of 10ng/ml ActivinA (R&D, 338-AC-050) incubation, and 1 day of 10ng/ml FGF9 incubation. On day8, the cells

were dissociated using TrypLE dissociation enzyme (Gibco, 12563011), and cell number was acquired. 75,000 cells/well were seeded on a 96-well ultralow-attachment plate (Corning, CLS7007) to form aggregates. The aggregates were formed in 3uM CHIR and 10ng/ml FGF9. On Day10, the media was changed to basal media with 10ng/ml FGF9. From Day13 to Day28, the aggregates were cultured in growth factor-free basal media. All differentiation steps were done using basal differentiation media (Advanced RPMI 1640 (Gibco, 12633020) + 1X Glutamax (Gibco, 35050079) + 1% Penicillin-Streptomycin (Invitrogen, 15070063).

Immunofluorescent Analyses

Before the immuno-detection was performed, frozen sections tissue was thawed at room temp for 10 minutes. Antigen retrieval was done in 1X Citrate Buffer pH 6.0 (Sigma) in a pressure cooker. The slides were washed with water and air dried for 5 min. The slides were incubated with 1.5% Seablock (ThermoFisher) in PBS + 0.25%TritonX block buffer for 1 hour at room temperature, and in primary antibody mixture (diluted in block buffer) at 4°C overnight. Primary antibodies used in the study are listed as follow: LHX1 (R&D, MAB2725,1:300), MAFB (R&D, MAB3810, 1:500), MAFB (Santa Cruz, sc-10022, 1:100), PAX8 (abcam, ab189249, 1:1000), KRT8/18 (DSHB, troma-1; 1:50), NPHS2 (abcam, ab50339, 1:10000), SYNPO (R&D, MAB8977, 1:300), TGFBR3 (R&D, AF-242-PB, 1:300), ANXA1 (Cell Signaling, 32934, 1:200), ARMH4/C14orf37 (Sigma Aldrich, HPA001789, 1:300), WT1 (abcam, ab89901, 1:1000), CUBN (Santa Cruz, sc-20607, 1:300), CDH1(Biosciences, 610182, 1:300), PDGFRB (abcam, ab32570, 1:500), VEGFR2 (Cell Signaling, 2479,1:150), GFRA3 (R&D, AF670, 1:300), PAX2 (R&D, AF3364, 1:500), F3 (R&D, AF2339, 1:500), PLVAP (BioRad, MCA2539GA,1:300), GATA3 (R&D, AF2605, 1:300), PECAM1 (BD Pharmingen, BDB550274, 1:300), EHD3 (Novus Biologicals, NBP2-31896, 1:300), FOXC2 (R&D, AF6989, 1:300). Secondary antibodies conjugated with AlexaFluor 488, 555, 594, and 647 were purchased from Molecular Probes. Slides were incubated with 1 μg/ml Hoechst 33342 (Molecular Probes) in PBS for 5 min to stain the nuclei. Sections were mounted in ProLong Gold Antifade Reagent (Life technologies) and imaged at 10X or 63X using the Leica SP8 confocal microscope.

In Situ Hybridization

We utilized RNAscope® Multiplex Fluorescent Reagent Kit v2 (Advanced Cell Diagnostics, Inc.) to perform fluorescent *in situ* hybridization. The slides were prepared as described above. Briefly, the tissues were treated with hydrogen peroxide and protease, then hybridized with RNAscope probes for 2 hours at 40°C using the HybEZ oven (Advanced Cell Diagnostics, Inc.). The probes were then amplified and detected with tyramide signal amplification fluorescence. To detect nuclei, the slides were incubated with 1 μg/ml Hoechst 33342 (Molecular Probes). The tissue was imaged at 63X using the Leica SP8 confocal microscope. The catalog numbers of probes from Advanced Cell Diagnostics, Inc. used in this work are listed as follow: *MAFB* (400801-C2), *RPS21* (511381-C3), *OLFM3* (549051-C3), *PLA2R1* (524581), *COL4A3* (461861) and *TNNT2* (518991-C3).

Single-Cell RNA-Sequencing and Analyses of Human Fetal Kidneys

Human kidney samples were embedded in 4% agarose block, and were sectioned to 300-μm thick sections using the vibratome (Leica VT1000S). The vibratome sections were further dissected manually to separate the outer cortex from the inner cortex. The specimens were enzymatically digested using collagenase A/pancreatin. Live single cells (DAPI- DRAQ5+) were selected using fluorescence-activated cell sorting (FACS) and were captured by microfluidic droplets using the Chromium 10x genomics platform as described previously (Lindström et al., 2018c). Quality control, mapping to reference genome and count table assembly of the libraries were performed using CellRanger 2.1 (10x Genomics) (Lindström et al., 2018c). The data is available at GEO accession number GSE124472.

The datasets from zone 1 and zone 2 cells were merged into one for initial analysis using the *MergeSeurat* function in Seurat package (Satija et al., 2015). The merged dataset was log-normalized using *NormalizeData* function. The *ScaleData* function was used to scale and center genes in the dataset, regressing the following variables against each gene: nUMI, nGene, saturation, and orig.ident. Quality control filtering was performed on the cells using the following criteria: saturation $\geq$70%, $\leq$5% mitochondrial genes. Principle components (PCs) were calculated using the *RunPCA* function, and statistically significant PCs ($p < 0.01$, Jackstraw criteria - Chung and Storey, 2015) were selected to use for clustering. We performed clustering using mclust package (Scrucca et al., 2016) with 41 PCs. Cluster assignments were initialized by hierarchical clustering (''hcVVV'' initialization in mclust). The number of clusters were decided based on Bayesien Information Criterion (BIC). Cell types were identified using known markers as well as GO term analyses of top differentially expressed genes.

Single-Cell RNA-Sequencing and Analyses of Human Kidney Organoids

Two DD 16 and two DD 28 kidney organoids of the same differentiation batch were dissociated by incubating with the Accumax™ Cell Dissociation Solution (Innovative Cell Technologies, Inc.) for 20min with gentle pipetting using P1000 tips. The dissociation enzyme was neutralized by autoMACS™ Running Buffer (Milteny Biotec), and the cells were centrifuged at 300 g for 5min. The pellet was resuspended in autoMACS™ Running Buffer (Milteny Biotec). The cell solution was run through a 40-μm cell strainer (Falcon) before live single cells (DAPI- DRAQ5+) were selected using FACS. The single cells were captured and subjected to single-cell sequencing using the Chromium 10x Genomics platform (Lindström et al., 2018c). The two DD 16 datasets and two DD 28 datasets were merged with the Seurat package using *MergeSeurat* function. Quality control and cluster finding were performed as described above for the human kidney datasets.

Pseudotime Reconstruction of Lineages

NPCs, early induced NPCs, early podocytes and podocytes were subset from the merged Zone1/Zone2 dataset using the Seurat package. We used the Monocle2 package to reconstruct differentiation trajectory (Qiu et al., 2017). Cells assigned by Monocle to the "proliferative" branch were selected against as described in (Lindström et al., 2018d). Non-proliferative cells were re-analyzed to build a developmental trajectory.

Differentially Expressed Gene Test between Two Podocyte Clusters

Differentially expressed genes from podocyte clusters in each dataset were obtained using the *FindMarkers* function in Seurat (Bimod test) (Satija et al., 2015). The following comparisons were performed: Week 15 (clusters 5 and 7) Zone 1 versus Zone2, Week 17 (clusters 3, 15 and 21) Zone 1 versus Zone 2, or Week 17 Late Podocyte (clusters 3 and 21) versus Organoid Podocyte (clusters 14, 19, 26 and 29) (representing "Podocyte Differences"). To account for "batch" variation due to tissue handling and origins of tissues, we selected non-epithelial clusters from the datasets (non-podocytes and PAX2-negative clusters – listed in table below), and performed differentially expressed gene test to obtain gene lists representing "Background Differences" (Table S2). Differentially expressed genes specific to podocyte were identified as "Podocyte Differences" genes absent from the "Background Differences" list, and were presented in volcano plots.

Samples	Clusters selected for "Podocyte Differences"	Clusters selected for "Background Differences"
Week 15	5, 7	6, 11, 14, 15, 16, 17, 18, 19, 20, 21
Week 17	3, 15, 21	6, 8, 12, 13, 14, 16, 17, 18, 19, 20
Organoid	14, 19, 26, 29	1, 3, 4, 5, 6, 11, 13, 16, 20, 23, 24, 25, 27

EP and LP Gene List Generation

To obtain the list of representative EP and LP genes (Figure S2C), we first inferred a set of genes that changed significantly across the differentiation trajectory using the differentialGeneTest function in Monocle2 (q-value < 0.05) (Qiu et al., 2017). We then filtered this list by selecting only genes correlated with known EP and LP markers: For a set of previously profiled markers (Figure S2D) we obtained the 50 genes with highest Pearson correlation with each one and selected, among the union of all correlated genes, the ones that were significant in the trajectory. Each resulting gene was visualized in a trajectory heatmap and manually curated to generate the lists of 158 EP genes and 104 LP genes.

Receptor-Ligand Analysis

To create a list of candidate receptor-ligand pairs between all clusters we used the list of receptor-ligand pairs proposed by Ramilowski et al., (2015). Given two clusters i and j, we calculated a score $S_k(i \rightarrow j)$ for each receptor-ligand pair (r_k, l_k) given by:

$S_k(i \rightarrow j) = p(i, l_k) \times p(j, r_k)$ where $p(i, g)$ is the proportion of single-cells in cluster i whose expression of gene g is nonzero. We set a significance cutoff $S > 0.25$ by visual inspection of the score distribution.

Hierarchical Clustering of Human Week 17 Clusters and Organoid Cell Clusters

Using the Seurat package, the Week 17 merged dataset was combined with the Kidney Organoid merged dataset (using *MergeSeurat* function) after identification of all clusters, and 70 PCs were calculated. To account for transcriptional differences due to origins of tissue, we examined all PCs using boxplots for distributions of cell loadings of each cluster; we removed PC2, which was homogeneous within one origin, but heterogeneous between human and organoid origins. Hierarchical clustering was then performed using the *BuildClusterTree* function in Seurat with PCs 1 to 70 excluding PC2.

SWNE Analysis of the Merged Human Week 17 and Organoid Cell Clusters

The Seurat object of merged human week 17 and organoid cells generated above was used as the input for SWNE (Wu et al., 2018a, 2018b). To select genes as input for SWNE (var.genes), we extracted the genes with highest loadings in each significant principal component of our joint analysis (PCs 1 to 70, excluding PC2). We sorted the squared loadings of each gene in decreasing order and kept the genes whose cumulative squared sum is smaller than 0.5. Our candidate gene list is the union of all significant genes across all principal components. Using var.genes, SWNE embedding was generated with 20-k factors. The plot was generated with alpha.exp = 1.6, snn.exp = 1, n_pull = 8, and 6 embedded factor genes (*SIX2, PDGFRB, POU3F3, PAX2, OLFM3*, and *MAFB*).

mRNA-Seq of MAFB-eGFP+ Cells from Kidney Organoids

Dd16 and dd28 kidney organoids from at least 3 differentiation batches were dissociated using the Accumax™ Cell Dissociation Solution (Innovative Cell Technologies, Inc.) and resuspended in autoMACS™ Running Buffer (Milteny Biotec) for FACS as described above. Live eGFP+ single cells were selected using stringent gate to separate the brightest eGFP+ DAPI- DRAQ5+ cells from eGFP- DAPI- DRAQ5+ cells. 50,0000 – 100,0000 cells collected from FACS were pelleted at 4°C, 2000 g for 10min, and resuspended in RLT buffer (RNeasy MicroKit, Qiagen). The RNeasy kit was used to purify RNA from the cells following the manufacturer's protocol.

mRNA-Seq libraries were prepared with KAPA Stranded mRNA-Seq Kit (Kapa Biosystems, #KK8420). The libraries were subsequently sequenced with Illumina NextSeq500 model with pair-end 75 bp setting.

mRNA-Seq of Human Fetal Renal Corpuscles

Human fetal kidneys of week 16-17 were minced and ground using the seal end of a 3-ml syringe plunger (BD Medical) on a 100-μm cell strainer (Falcon). Dissociated tissue passing through the strainer was collected in DMEM, and the flow-through was filtered using a 70-μm cell strainer (Falcon). Renal corpuscles trapped on the 70-μm strainer were collected in DMEM, concentrated by centrifuging at 1000 g for 5 min, and lysed in RLT buffer for RNA extraction (RNeasy MicroKit, Qiagen). The 70-μm strainer flow-through portion was also collected in RLT buffer for mRNA profiling. mRNA-Seq libraries were prepared as described above.

mRNA-Seq of Immortalized Podocytes

Human immortalized podocytes were obtained from Dr. Moin Saleem's group (University of Bristol) and cultured following the existing protocols (Saleem et al., 2002; Ni et al., 2012). Cells were collected before thermoswitch (cultured at 33°C) and after thermoswitch (cultured at 37°C) in RLT buffer (RNeasy MicroKit, Qiagen) for RNA extraction. mRNA-Seq libraries were prepared as described above.

mRNA-Seq Data Analysis

mRNA-Seq reads were aligned with TopHat2 (Kim et al., 2013; Trapnell et al., 2009) to hg38 assembly. The aligned reads were quantified with Partek Genomics Suite software, version 6.6 (St. Louis, MO, USA) to obtain both RPKM and counts at gene level. TPM was calculated by dividing the RPKM by the mapping ratio of the library to exon regions of the genome. To identify differentially expressed genes, count tables of the two groups of data being compared were first processed through DESeq2 (Love et al., 2014) to obtain the p values from negative binomial tests which evaluates the significance of difference by read counts. Next, the TPM tables of the same samples were used to calculate the two-sample independent t-test p values. Both p values were used in screening for differentially expressed genes ($p < 0.05$ in both cases). Only genes with TPM > 5 in the more highly expressed samples were selected. Top 2000 most variably expressed genes of all samples were selected and their TPM values were plotted with 'heatmap2' in the 'gplot' package of R.

Gene-List GO-Term Queries

Differentially expressed genes or gene module lists were queried by ToppGene (Chen et al., 2009) identifying Biological Processes and Coexpression Atlas.

Glomerular Disease-Related Gene Expression Analysis

Genes associated with human ''glomerulosclerosis'' and ''glomerulopathy'' were obtained from the Online Mendelian Inheritance in Man (OMIM) database and Lepori et al., (2018). The average expression levels of OMIM genes were calculated using the *AverageExpression* function in Seurat for the following cell populations: Week 17 early and late podocyte, Week 17 mesangial cells, Week 17 glomerular endothelial cells, Organoid early and late podocytes. Genes with average expression higher than 0 were presented using the *DotPlot* function in Seurat.

Analysis of Published scRNASeq Dataset

Datasets from the Czerniecki et al. (2018) and Wu et al. (2018a, 2018b) studies were acquired through GEO (GSE109718 and GSE118184, respectively). The Seurat package was used to obtain feature plots displaying expression of genes of interest.

Analysis of Microarray Datasets

Microarray data was acquired through GEO (GSE17142, GSE17143, GSE17145). The Oligo package (Carvalho et al., 2010) was used to process the CEL files. The Limma package (Ritchie et al., 2015) was used to normalize the data sets and perform statistical inference. To find differentially expressed genes between two given groups, we used the following threshold: DEseq value > 6, fold change > 3 and p-value < 0.01.

Renal Capsule Transplant

The procedure was adapted from (Yoshimura et al., 2017). Week 8–12 NOD.CB17-Prkdc<SCID>/J mice were anesthetized with Ketamine/Xylazine. Surgery site at the dorsal flank was shaved and swabbed with Proviodine/alcohol. An 8-10 mm incision was made, and the fascia was incised before the kidney was externalized. The kidney capsule was kept moistened with sterile saline during the procedure. A small incision was made in the outer membrane of the renal capsule at the caudal end, using a sharp 24g needle and the sub capsular space is flushed with 1ml of basal differentiation media using a blunted 24g needle 30g needle (B30-50, Strategic Applications, Inc.) attached to a 1 ml syringe. Two agarose rods (2mm long, 0.5mm diameter) were pushed into the sub capsular space in the shape of an open V using forceps. A 20g indwelling needle (SURFLO® PTFE I.V. Catheter needle, TESR-OX2025CA, VWR) attached to a 1 ml syringe and draw up 3-4 dd13-14 organoids basal differentiation media into the needle. The indwelling needle was inserted under the renal capsule to place organoids between the agarose rods. The capsule incision was cauterized, and the kidney was replaced into the retroperitoneum. The muscle layer was sutured, and the skin was closed with wound clips.

Intravital Multiphoton Microscopy

NOD SCID mice were anesthetized with isoflurane (3% in induction chamber and 1.5-1.8% for maintenance through nasal cone). Alexa594-conjugated bovine serum albumin (ThermoFisher) was administered iv. by retro-orbital injections to label the circulating plasma (30μL iv. bolus from 10 μg/ml stock solution). Subcapsular organoid implants in left kidney were exteriorized through a 8-10 mm incision under sterile conditions. In all procedures, body temperature was maintained by using a homeothermic blanket (Harvard Apparatus, Holliston, MA). The mouse was placed on the stage of an inverted microscope with the exposed kidney placed in a coverslip-bottomed chamber bathed in normal saline.

Image acquisition of intact organoids was performed *in vivo* using a Leica SP8 DIVE multiphoton confocal fluorescence imaging system (Leica Microsystems) powered by a Coherent Discovery laser system at 860 nm excitation (Coherent) and a DMI8 inverted microscope's external Leica 4Tune spectral hybrid detectors (emission at 530±10nm for eGFP and 600nm for Alexa594-Albumin). Images were acquired in 12-bit, 512×512 pixel using a 40X Leica water immersion objective (NA 1.1). (Hackl et al., 2013; Kang et al., 2006). All animal protocols were approved by the Institutional Animal Care and Use of Committee at the University of Southern California.

DATA AND CODE AVAILABILITY

The bulk and single-cell RNA sequencing datasets are available under GEO accession numbers: GSE127344, GSE124392, and GSE124472.